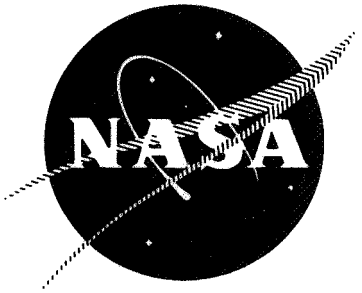

NASA CR-120968

R-8973-3

INJECTOR DESIGN GUIDELINES FOR GAS/LIQUID PROPELLANT SYSTEMS

By

A. Y. Falk

R. J. Burick

ROCKETDYNE
A DIVISION OF ROCKWELL INTERNATIONAL
6633 CANOGA AVENUE, CANOGA PARK, CALIFORNIA

prepared for

NATIONAL AERONAUTICS AND SPACE ADMINISTRATION

NASA-Lewis Research Center
NAS3-12051
Larry H. Gordon, Project Manager

NOTICE

This report was prepared as an account of Government-sponsored work. Neither the United States, nor the National Aeronautics and Space Administration (NASA), nor any person acting on behalf of NASA:

A. Makes any warranty of representation, expressed or implied, with respect to the accuracy, completeness, or usefulness of the information contained in this report, or that the use of any information, apparatus, method, or process disclosed in this report may not infringe privately-owned rights; or

B. Assumes any liabilities with respect to the use of, or for damages resulting from the use of, any information, apparatus, method or process disclosed in this report.

As used above, "person acting on behalf of NASA" includes any employee or contractor of NASA, or employee of such contractor, to the extent that such employee or contractor of NASA or employee of such contractor prepares, disseminates, or provides access to any information pursuant to his employment or contract with NASA, or his employment with such contractor.

Requests for copies of this report should be referred to

National Aeronautics and Space Administration
Scientific and Technical Information Facility
P.O. Box 33
College Park, Md. 20740

1. Report No.	2. Government Accession No.	3. Recipient's Catalog No.
NASA CR-120968		

4. Title and Subtitle	5. Report Date
INJECTOR DESIGN GUIDELINES FOR GAS/LIQUID PROPELLANT SYSTEMS	May 1973
	6. Performing Organization Code
7. Author(s)	8. Performing Organization Report No.
A. Y. Falk and R. J. Burick	R-8973-3
	10. Work Unit No.
9. Performing Organization Name and Address	
Rocketdyne, a division of Rockwell International Canoga Park, California 91304	11. Contract or Grant No. NAS3-12051
	13. Type of Report and Period Covered
12. Sponsoring Agency Name and Address	Contractor Report
National Aeronautics and Space Administration Washington, D.C. 20546	14. Sponsoring Agency Code

15. Supplementary Notes

Project Manager, Larry H. Gordon, NASA-Lewis Research Center, Cleveland, Ohio

16. Abstract

This report provides injector design guidelines for gas/liquid propellant systems. Information for this report was obtained from a 30-month applied research program (Contract NAS3-12051) encompassing an analytical, design, and experimental effort to relate injector design parameters to simultaneous attainment of high performance and component (injector/thrust chamber) compatibility for gas/liquid space storable propellants. The gas/liquid propellant combination studied was FLOX (82.6% F_2)/ ambient temperature gaseous methane. The injector patterns characterized were like (self)-impinging doublet and circular coaxial.

Design criteria that provide for simultaneous attainment of high performance and chamber compatibility are presented for both injector types. Parametric data are presented that are applicable for the design of circular coaxial and like-doublet injectors that operate with design parameters similar to those employed in the work reported herein. However, caution should be exercised when applying these data to propellant combinations whose elements operate in ranges considerably different from those employed in this study. To obtain good quantitative design guidance in these cases, the recommended approach would be to apply the cold-flow propellant distribution measurement techniques and combustion models developed and verified under Contract NAS3-12051 directly to the propellant and design requirements of interest.

To illustrate the use of the design guidelines presented herein for gas/liquid injector design, design examples are presented for a liquid oxygen/gaseous propane injector operating at a nominal chamber pressure of 150 psia (MR = 2.9; sea level thrust = 5000 lbf).

17. Key Words (Suggested by Author(s))	18. Distribution Statement
Coaxial Injector Like-Doublet Injector Combustion Performance Injector Mixing Heat Flux Profile	

19. Security Classif. (of this report)	20. Security Classif. (of this page)	21. No. of Pages	22. Price*
Unclassified	Unclassified	90	

* For sale by the National Technical Information Service, Springfield, Virginia 22151

FOREWORD

The work described herein was conducted for the NASA-Lewis Research Center, Cleveland, Ohio, by the Advanced Programs Department of Rocketdyne, a division of Rockwell International. The study was conducted in accordance with Contract NAS3-12051, Rocketdyne G.O. 09222.

This report (NASA CR-120968; R-8973-3), which summarizes and demonstrates the use of injector-thrust chamber design criteria/techniques developed under Contract NAS3-12051, is one of three reports emerging from the subject contract. Separate reports describing the like doublet (NASA CR-120935; R-8973-1) and coaxial injector (NASA CR-120936; R-8973-2) characterization portions of the contract also were published.

Mr. L. H. Gordon of the NASA-Lewis Research Center served as NASA Technical Project Manager. The Rocketdyne Program Manager was Mr. H. G. Diem. Technical guidance of the program was provided by Mr. S. D. Clapp and Dr. D. T. Campbell.

Important contributions to the conduct of the program were made by the following Rocketdyne personnel: R. R. Doubleday, J. T. Sabol, D. Zwald, and R. Barnsdale.

CONTENTS

ABSTRACT

This report provides injector design guidelines for gas/liquid propellant systems. Information for this report was obtained from a 30-month applied research program (Contract NAS3-12051) encompassing an analytical, design, and experimental effort to relate injector design parameters to simultaneous attainment of high performance and component (injector/thrust chamber) compatibility for gas/liquid space storable propellants. The gas/liquid propellant combination studied was FLOX (82.6% F_2)/ambient temperature gaseous methane. The injector patterns characterized were like (self)-impinging doublet and circular coaxial.

Design criteria that provide for simultaneous attainment of high performance and chamber compatibility are presented for both injector types. Parametric data are presented that are applicable for the design of circular coaxial and like-doublet injectors that operate with design parameters similar to those employed in the work reported herein. However, caution should be exercised when applying these data to propellant combinations whose elements operate in ranges considerably different from those employed in this study. To obtain good quantitative design guidance in these cases, the recommended approach would be to apply the cold-flow propellant distribution measurement techniques and combustion models developed and verified under Contract NAS3-12051 directly to the propellant and design requirements of interest.

To illustrate the use of the design guidelines presented herein for gas/liquid injector design, design examples are presented for a liquid oxygen/gaseous propane injector operating at a nominal chamber pressure of 150 psia (MR = 2.9; sea level thrust = 5000 lbf).

ILLUSTRATIONS

TABLES

1.0 SUMMARY

This report presents injector design guidelines for gas/liquid propellant systems. Design information is provided for simultaneous attainment of high performance and chamber compatibility. The design criteria (guidelines) presented are based on data from a 30-month program of analysis, design, and experiment conducted to relate injector/thrust chamber design parameters to simultaneous attainment of high performance and component compatibility for a FLOX/gaseous methane propulsion system (Ref. 1 and 2). Design conditions were for sea level thrust of 3000 pounds at a chamber pressure of 500 psia (MR = 5.25). The gas/liquid injector patterns characterized utilized like (self)-impinging doublet and circular coaxial elements. Design criteria were established (parametrically, based on combined cold-flow and hot-fire data) to allow for subsequent extrapolation to other advanced gas/liquid propellant combinations and operating conditions.

The effects of pertinent design and operating variables on mixing/atomization for the like-doublet/coaxial element are discussed in detail herein.

Mixing for the like-doublet element is primarily a function of its geometric design parameters (fan spacing, fan inclination angle, etc). Propellant momentum ratio is of secondary importance. Considerable interelement mixing (i.e., a high-element density) is required to achieve high performance with the like-doublet pattern. Atomization is primarily a function of the orifice size and injection velocity. However, use of the injected gaseous propellant to aid in atomization of the liquid propellant and combustion gas effects on "secondary atomization" also can be appreciable. Control of peripheral zone propellant mass and mixture ratio distribution for chamber compatibility can be achieved by spacing of the fuel and oxidizer fans and by proper alignment of these fans in relation to the chamber wall.

Mixing for the coaxial element can be correlated as a function of a single parameter, $(\rho_g V_g)^2/MR \cdot V_L$, which is in turn a function of pertinent element design and operating variables. Interelement mixing is of less importance for the coaxial element than for impinging jet elements. Atomization characteristics of this element type can also be correlated as a function of element design and operating variables $((V_g - V_L)/MR \cdot V_L)$. Control of peripheral zone mass and mixture ratio distribution for chamber compatibility is most efficiently attained with the coaxial element by means of boundary layer coolant.

Information is contained in this report to permit design of high-performance, chamber-compatible gas/liquid like-doublet/circular coaxial injectors. This information was developed on Contract NAS3-12051 (Space Storable Propellant Performance Program). Design examples are provided to illustrate the use of the data presented herein in the design of like-doublet and coaxial ($LOX/C_3H_8(g)$) injectors.

The hot-fire and cold-flow data from Contract NAS3-12051 can be employed as guidelines for design of high-performance chamber-compatible injectors for other gas/liquid propellant combinations. *However, caution should be exercised when applying these data to propellant combinations whose elements operate in*

ranges considerably different than those employed in this study. To obtain good quantitative design guidance in these cases, the recommended approach would be to apply the cold-flow propellant distribution measurement techniques and combustion models developed and verified under Contract NAS3-12051 directly to the propellant and design requirements of interest.

2.0 INTRODUCTION

The primary purpose of this report is to provide injector design guidelines for gas/liquid propellant systems. Design information is provided for simultaneous attainment of high performance and chamber compatibility. Prerequisites for high performance are uniform propellant mixing and good atomization. Chamber heat flux/erosion can be controlled by design techniques to ensure acceptable peripheral zone propellant mass and mixture ratio distributions. The injector patterns considered are like (self)-impinging doublet and circular coaxial.

Guidelines for design of high-performance, like-doublet, and circular coaxial injectors are presented in Section 3.0 of this report under separate headings (3.1--Like Doublet; 3.2--Coaxial). Guidelines for injector element design to achieve chamber compatibility with minimal performance losses due to propellant mass and mixture ratio control (zoning) near the chamber wall are presented in Section 4.0. In both cases, experimental results from both cold-flow mass and mixture ratio distribution and hot-fire performance/heat flux measurements were used as a basis for the recommended design guidelines.

Conclusions and recommendations about cold-flow injector modeling techniques, and the application of the design guidelines presented in Sections 3.0 and 4.0 to propellant combinations whose elements operate in ranges considerably different than those upon which they were based, are presented in Section 5.0.

A design example illustrating the use of the design guidelines presented herein is included as Section 6.0. Both injector types are considered.

3.0 PERFORMANCE GUIDELINES

Injector design criteria for simultaneous attainment of high propellant mixing uniformity and good atomization are a prerequisite for high performance. Experimental results from both cold-flow mass and mixture ratio distribution and hot-fire tests were used as a basis for the recommended design guidelines. Guidelines for design of high performing, like-doublet, and coaxial elements and/or injectors are presented in this section of the report under separate headings.

3.1 LIKE-DOUBLET ELEMENT PATTERN

Definition of the like-doublet element configuration, range of experimental data, propellant mixing characteristics, propellant atomization characteristics, and interelement considerations are presented herein for the like-doublet element pattern.

3.1.1 Element Configuration

A schematic representation of a like-doublet element (element = matched pair of fuel and oxidizer doublets) is presented in Fig.1 . The geometric factors affecting propellant distribution (mixing)/atomization for this element type are illustrated in this figure. Mixing for the like-doublet element is primarily a function of its geometric design parameters (fan spacing, fan inclination angle, etc.). Propellant momentum ratio is of secondary importance.

3.1.2 Range of Experimental Data

Selection of zero fan spacing (S) and impingement angle (β) as optimum was based on previous studies with liquid/liquid propellant systems (Ref. 3, 4, 6, and 7). Specific design considerations for the full-scale injectors of Contract NAS3-12051 for which these data were generated (i.e., number of elements required for simultaneous attainment of high performance and control of injector-chamber compatibility, available injector face area, orifice diameters required for good atomization/reasonable injector pressure drops, etc.) limited the range of usable intra-element spacing ($\sim$0.15 to 0.30 inch) and orifice diameters ($\sim$0.030 to 0.09 inch). Intra-element spacings of 0.15 and 0.20 inch were employed. Selection of these values were based on previous experience with liquid/liquid propellant systems. Those results indicate that, in general, optimization of the intra-element spacing (Y) and fan inclination angle (α) are interrelated. However, in the range of practical interest for Contract NAS3-12051, intraelement spacing effects have been negligible. *Fan inclination angle (α) and propellant momentum ratio were, therefore, selected as the primary test variables.* Previous experience with liquid/liquid like-doublet elements indicated that both of these variables influence mixing and lend themselves to optimization.

During *single-element* cold-flow mixing experiments, the fan inclination angle (α) was varied in 15-degree increments from 0 to 30 degrees at a constant momentum ratio (ℓ/g) of 0.34. Propellant momentum ratio was varied from about 0.25 to 2.0 at a constant fan inclination angle of 15 degrees. Momentum ratio was varied by varying mixture ratio/chamber pressure with a fixed-element configuration and, alternatively, by successive enlargement of the gas orifice diameter

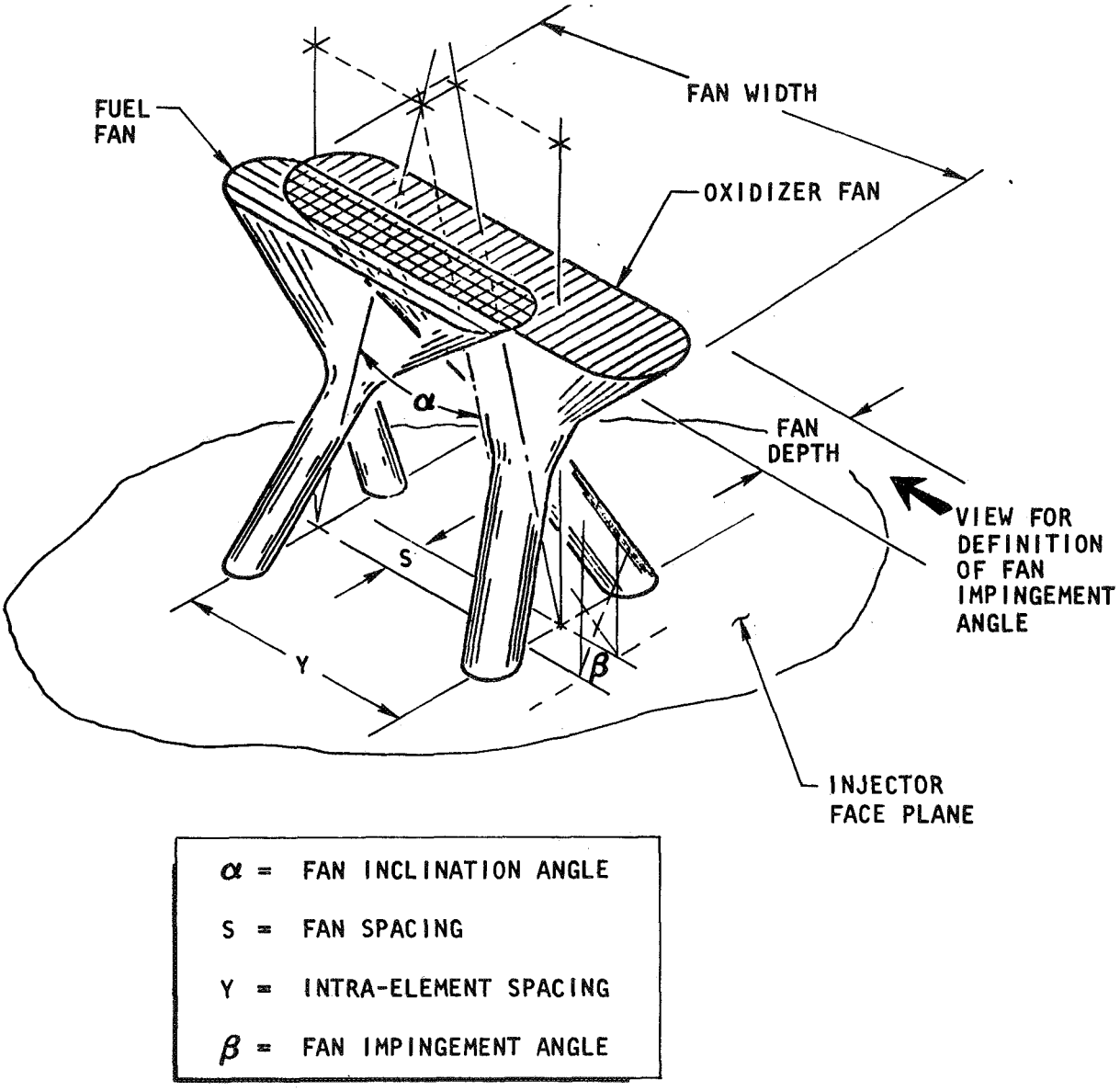

Figure 1. Schematic Representation of Like-Doublet Element Showing Geometric Factors Affecting Propellant Mixing/Atomization (Element = Pair of Fuel and Oxidizer Doublets)

at constant mixture ratio and chamber pressure. Most of the tests were conducted at a mixture ratio of approximately five. Two element configurations were employed: one with d_ℓ = 0.037 inch, d_g = 0.043 inch, and intra-element spacing (Y) = 0.15 inch; the second with d_ℓ = 0.052 inch, Y = 0.20 inch, and d_g of 0.055, 0.082, and 0.104 inch ($0.50 \leq d_\ell/d_g \leq 0.95$). A jet impingement angle (included angle) of 60 degrees was used for all gas/liquid doublets, and free stream and orifice L/D ratios of approximately 4 and 10, respectively, were employed on all of the like-doublet elements.

Table I presents the range of variables that were investigated during the high-performance, like-doublet element (cold-flow) mixing tests. Optimum values for each parameter (where applicable) are noted.

The cold-flow mixing experiments were conducted in a pressurized environment to model the hot-fire gas/liquid flowfield of interest. Propellant simulants were water (FLOX) and GN_2 (methane). A description of the pressurized gas/liquid cold-flow mixing facility and its operating procedures are presented in Ref. 1. To simulate operation at a given chamber pressure and mixture ratio, hot-fire injected gas momentum flux, propellant momentum ratio, and mixture ratio were matched.

3.1.3 Mixing Characteristics

Fan Inclination Angle Effects. The effect of fan inclination angle on propellant mixing for high performance (zero fan spacing) like-doublet elements is shown in Fig. 2. Element design and operating parameters are noted in the figure. The effect of fan inclination angle on propellant mixing uniformity for the subject element type (S = 0) is quite small. E_m and $\eta_{c^*,\,mix}$ for FLOX (82.6% F_2)/CH_4 are relatively independent of α(E_m and $\eta_{c^*,\,mix}$ are defined below). Because of the relative insensitivity of E_m to α seen in these results, selection of a specific fan inclination angle as optimum required further analysis of the distribution data.

The c* efficiency due to propellant mixing ($\eta_{c^*,\,mix}$) is a function of the mixing uniformity index (E_m), propellant combination, and the overall injected mixture ratio, $\eta_{c^*,\,mix}$, is defined below:

$\eta_{c^*,\,mix}$ = the c* efficiency which would be obtained if propellant vaporization were entirely complete, and the only losses were caused by nonuniform propellant mixing

$$= \frac{\sum_{i}^{n} MF_i c^*_i}{c^*_{theo}} \qquad (1)$$

TABLE I. RANGE OF VARIABLES FOR HIGH-PERFORMANCE LIKE-DOUBLET ELEMENT MIXING TESTS

Parameter	Symbol	Range	Optimum Value
Fan Spacing, inches	S	0	0
Impingement Angle, degrees	β	0	0
Intra-element Spacing, inches	γ	0.15 and 0.20	0.15/0.20
Fan Inclination Angle, degrees	α	0, 15, and 30	15
Propellant Momentum Ratio (liquid-to-gas)	M	0.25 to 2.0	0.7 to 1.5
Mixture Ratio	MR	5 to 9	--
Liquid Orifice Diameter, inches	d_ℓ	0.037 and 0.052	--
Gas Orifice Diameter, inches	d_g	0.043, 0.055, 0.082	--
Orifice Diameter Ratio	d_ℓ/d_g	0.50 to 0.95	--

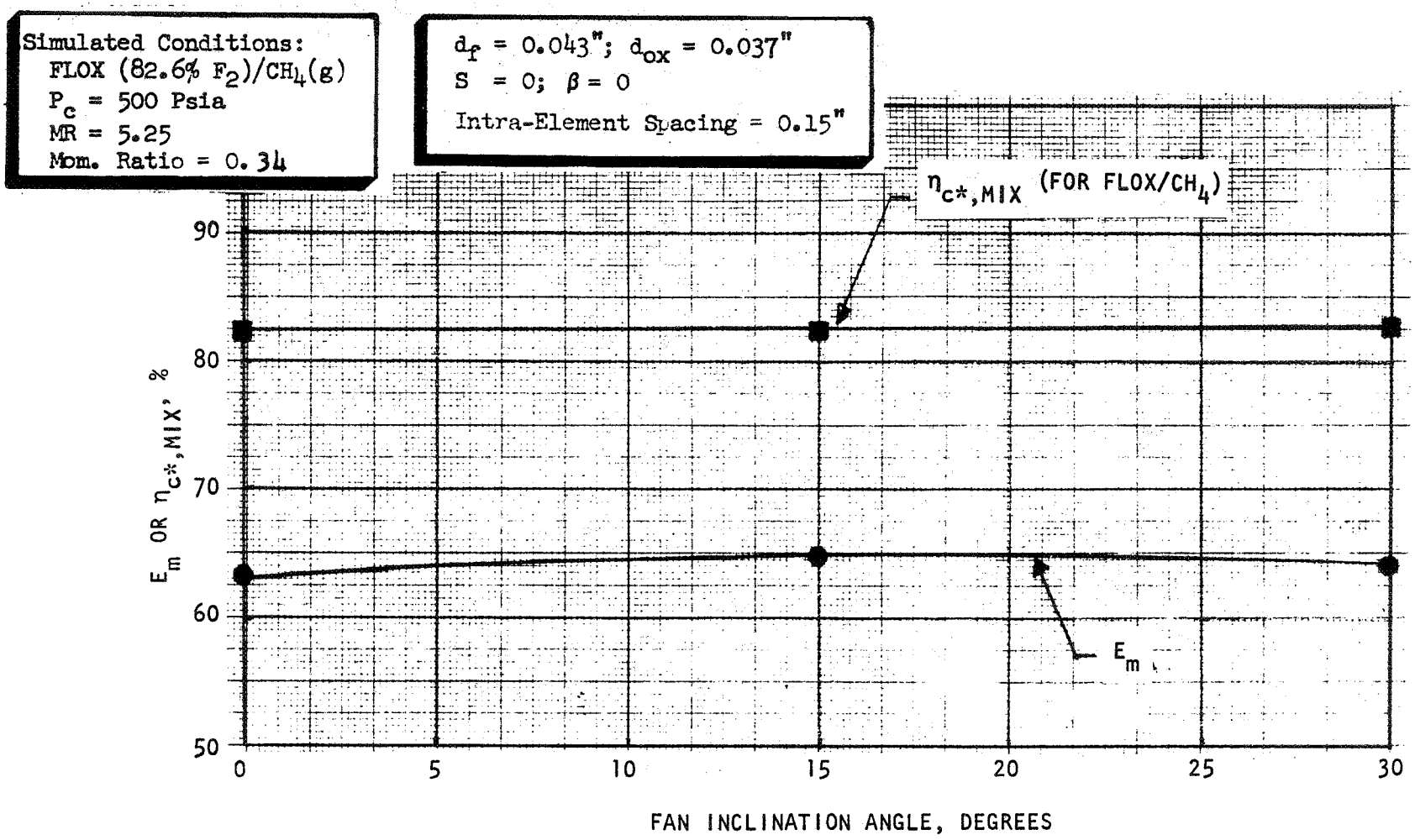

Figure 2. Effect of Fan Inclination Angle (α) on Mixing for High Performance (S = 0) Like-Doublet Single Element

where

MF_i = the mass fraction in the individual stream being considered

c^*_i = theoretical c* corresponding to the mixture ratio of the local stream

c^*_{theo} = theoretical c* corresponding to the overall mixture ratio

As shown by the above equation, $\eta_{c^*,\,mix}$ is simply the sum of the mass weighted c* contributions of each individual stream tube divided by the c* theoretically attainable at the overall injected mixture ratio.

The mixing quality can be expressed by an index, E_m, which defines the mass weighted deviation of local mixture ratio from initially injected overall mixture ratio. The index, E_m, was developed by Rupe (Ref. 8) and is defined below:

$$E_m = \left[1 - \left(\sum_i^n MF_i \frac{(R - r_i)}{R} + \sum_i^n MF_i \frac{(R-\bar{r}_i)}{R-1}\right)\right] 100 \qquad (2)$$

where

E_m = mixing index

MF_i = mass fraction in the stream tube

R = ratio of total oxidizer mass to total oxidizer and fuel mass

r_i = ratio of oxidizer mass to total oxidizer and fuel mass is an individual stream tube for $r_i < R$

$\bar{r}_i$ = ratio of oxidizer mass to total oxidizer and fuel mass in an individual stream tube for $r_i > R$

The foregoing expression for the distribution index is not universal because $\eta_{c^*,\,mix}$ is also functionally related to the propellant combination and overall injected mixture ratio.

Examination of local values of the propellant mass flux distribution (for the tests conducted to define fan inclination angle effects on mixing) provided criteria for selection of a specific fan inclination angle as optimum. These data indicated that, as the fan inclination angle was increased, the mass flux plots became more nonuniform/unsymmetrical. Since all appear to yield nearly the same mixing uniformity (Fig. 2), a low fan impingement angle would be favored because of the more uniform overall maxx flux distribution. The effect of the gas on the resultant distribution is quite pronounced at high fan inclination angles. Propellant distribution is controlled by the gas at high fan inclination angles, especially with low liquid-to-gas momentum ratios.

From injector design/fabrication considerations, a relatively low fan inclination angle is also favorable. A high fan inclination angle considerably increases the design/drilling complexity of the injector. It also increases the

required area per element and decreases the number of elements that can be placed in a fixed area. Previous experience with liquid/liquid propellant systems indicate that $\alpha = 0$ is not optimum. For these reasons, a fan inclination angle of 15 degrees was selected as optimum.

Propellant Momentum Ratio Effects. The effect of momentum ratio (liquid-to-gas) on mixing for a zero fan spacing and 15-degree fan inclination angle, like-doublet, single element is shown in Fig. 3 . Cold-flow test conditions and element design parameters are noted in this figure. Increasing the momentum ratio from 0.3 to 0.6 increases the mixing index E_m by approximately 4.5% (64.4 to 68.6). E_m is relatively independent of momentum ratio for momentum ratios $\geq$0.6 over the range investigated (0.3 to 2.0).

A fan inclination angle of 15 degrees in conjunction with an oxidizer-to-fuel momentum ratio of 0.7 to 1.5 was chosen as optimum. Hot-fire variation of propellant momentum ratio substantiated the result presented in Fig. 3 (Ref. 1).

During hot-fire and cold-flow experiments momentum ratio was varied by: (1) throttling at constant mixture ratio, (2) varying mixture ratio at constant chamber pressure, and (3) successive enlargement of the fuel/oxidizer orifice diameters. These data suggested that over the range of experimental data contained herein, all methods for variation of momentum ratio produced equivalent parametric results.

3.1.4 Atomization Characteristics

Hot-fire mean drop sizes for liquid/liquid like-doublet elements can be estimated using the following equation (Ref. 3):

$$D_{30} = \frac{25{,}400}{2.64\sqrt{\frac{V_j}{D_j}} + K\left(\frac{\rho_{actual}}{\rho_{ref}}\right)^{1/4}\left|(\Delta V)\right|} \qquad (3)$$

where

D_{30} = volume-mean-diameter of resulting droplets, microns

D_j = liquid orifice diameter, inches

V_j = liquid injection velocity, ft/sec

$K = 0.97 \times \left[\left(\frac{\mu\sigma}{\rho}\right)_{\text{n-heptane}} \Big/ \left(\frac{\mu\sigma}{\rho}\right)_{\text{propellant}}\right]^{1/4}$

$\left(\frac{\rho_{actual}}{\rho_{ref}}\right)$ = ratio of actual to reference gas density (ρ_{ref} = 1.06 g/ℓ)

$\Delta V = (V_g - V_j)$ = relative velocity difference between combustion gas and liquid jet, ft/sec

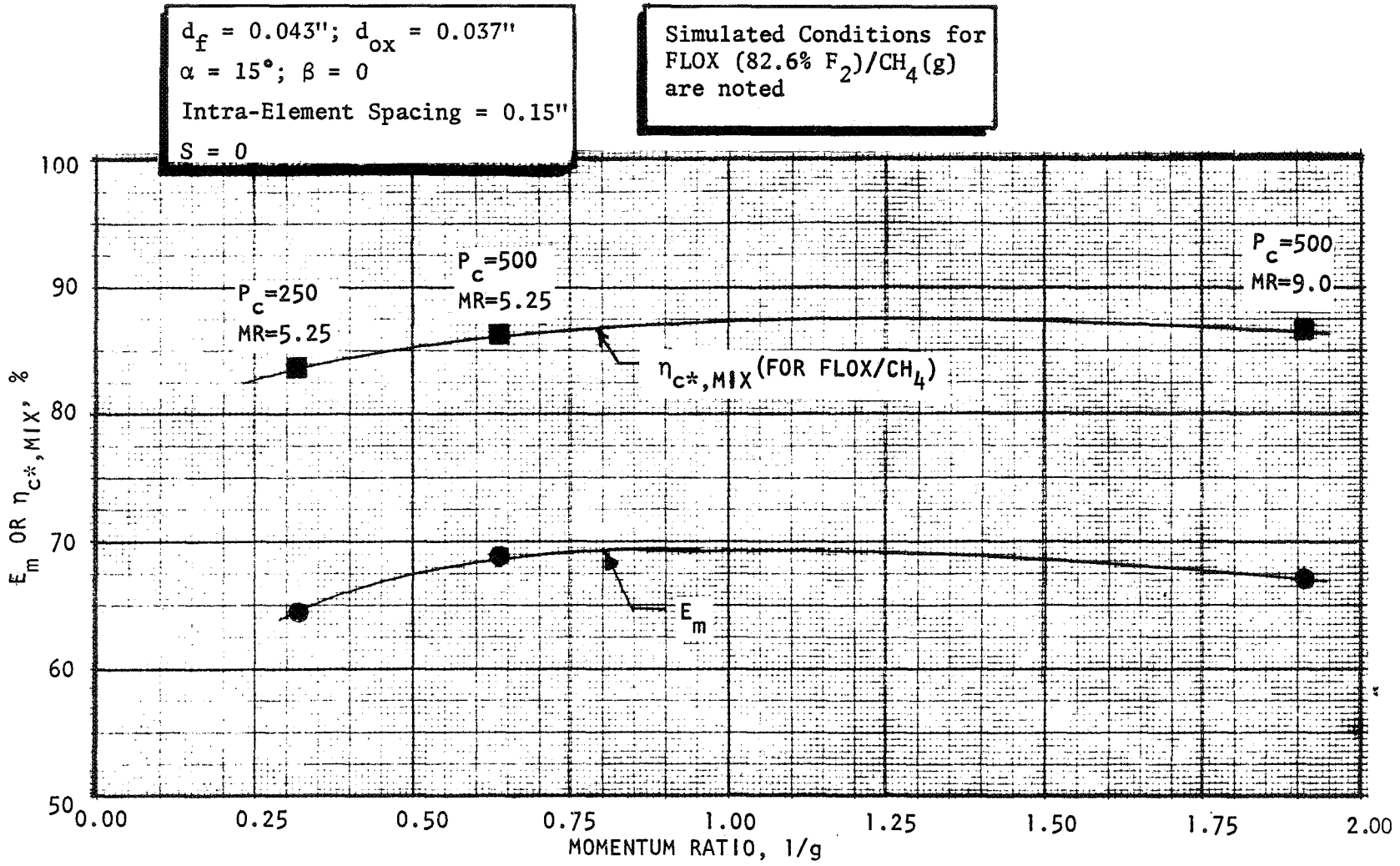

Figure 3. Effect of Momentum Ratio (Liquid-to-Gas) on Mixing for Zero Fan Spacing Like-Doublet Single Element

The effective combustion gas velocity (V_g) is peculiar to the propellant combination and, at present, no a priori method has been established for its prediction. However, an empirical correlation expressing V_g as a function of chamber contraction ratio (ε_c = 2,3, or 4) was found to be quite effective in correlating the hot-fire data obtained under Contracts NAS3-11199 (Ref. 3) and NAS3-12051 (Ref. 1). This expression is given below:

$$V_g = \frac{640}{\varepsilon_c} \tag{4}$$

where

ε_c = chamber contraction ratio.

To predict the vaporization-limited c* efficiency for a system using existing combustion models, the distribution of the droplets about the median D_{30} must be known as well as D_{30}. A "like-doublet drop size distribution" obtained from Ref. 4 must be employed in the combustion model analysis. This information is presented in Fig. 4 .

3.1.5 Interelement Considerations

Since single-element mixing levels are low ($E_m \cong 60$ to 70), it was recognized early in the program that substantial interelement mixing would be required in a full-scale, like-doublet injector to achieve high performance. Consequently, cold-flow mixing experiments were conducted to provide this information.

Element density/interaction effects on mixing for performance optimized like-doublet elements are shown in Fig. 5 . E_m and cold-flow mixing c* efficiency (for FLOX(82.6%)F_2/CH_4) are shown plotted as a function of element density in this figure. As noted, high-element density is required for high mixing uniformity. This figure defines the element density required to achieve any reasonable desired level of mixing.

The data in Fig. 5 can be employed in conjunction with Fig. 6 to determine $\eta_{c^*,\ mix}$ for FLOX/CH_4 or FLOX/B_2H_6 propellant combinations. For propellant combinations other than these, Eq. 1 can be employed in conjunction with a multi-streamtube analysis to determine $\eta_{c^*,\ mix}$ as a function of E_m.

Several general points should be made about the information presented in Fig. 6. First, performance losses for a given level of mixing uniformity (E_m) are substantially greater for one of the propellant combinations (FLOX/CH_4) than for the other. In general, performance losses due to nonuniform mixing are substantially greater for FLOX/light hydrocarbon systems than for most propellant combinations. Secondly, for a given level of E_m, performance losses for mixture ratios $\geq$ the optimum value are, in general, greater than those for mixture ratios $\leq$ the optimum value.

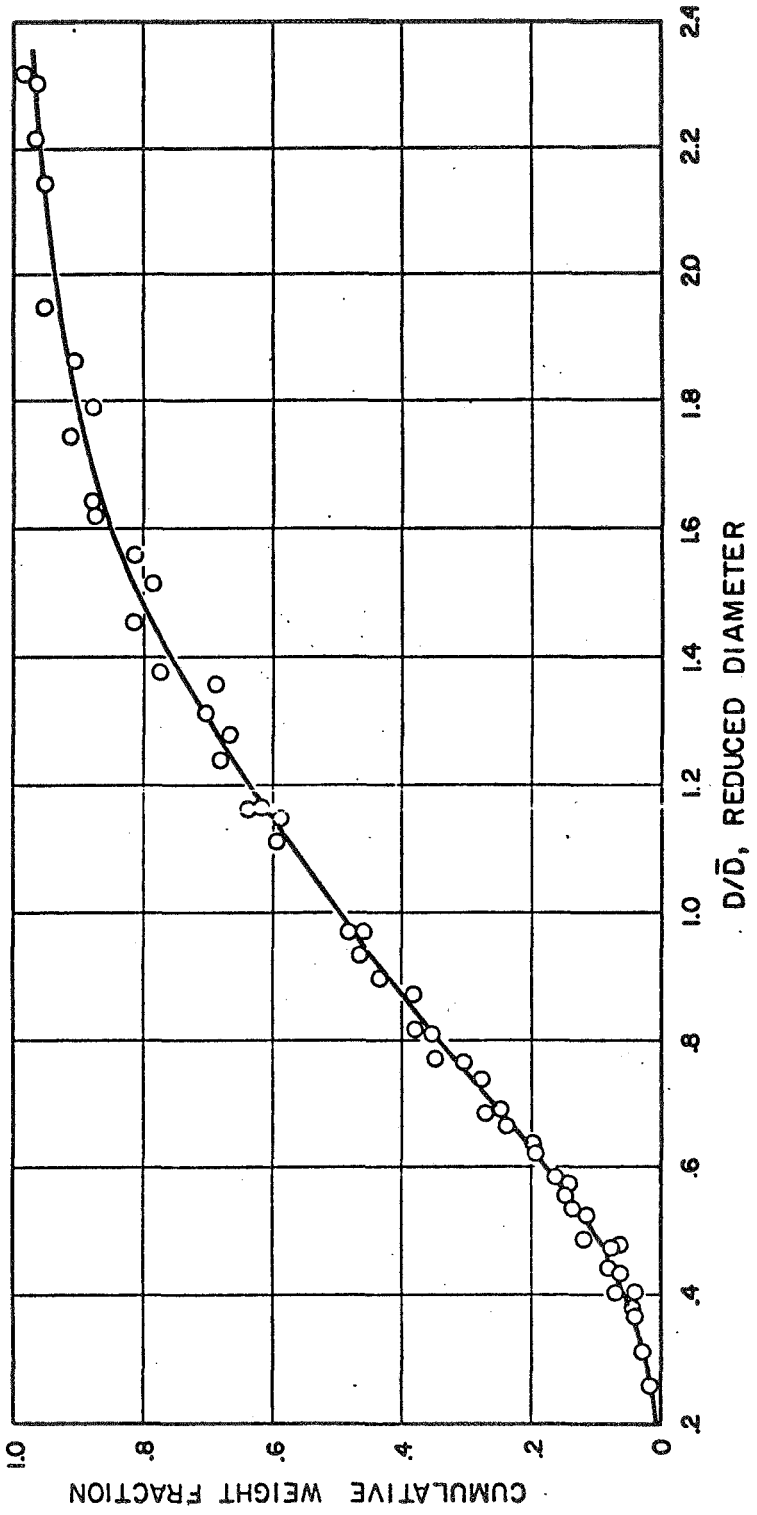

Figure 4. Normalized Particle Size Distribution Curve for Like Doublets With Zero Spacing

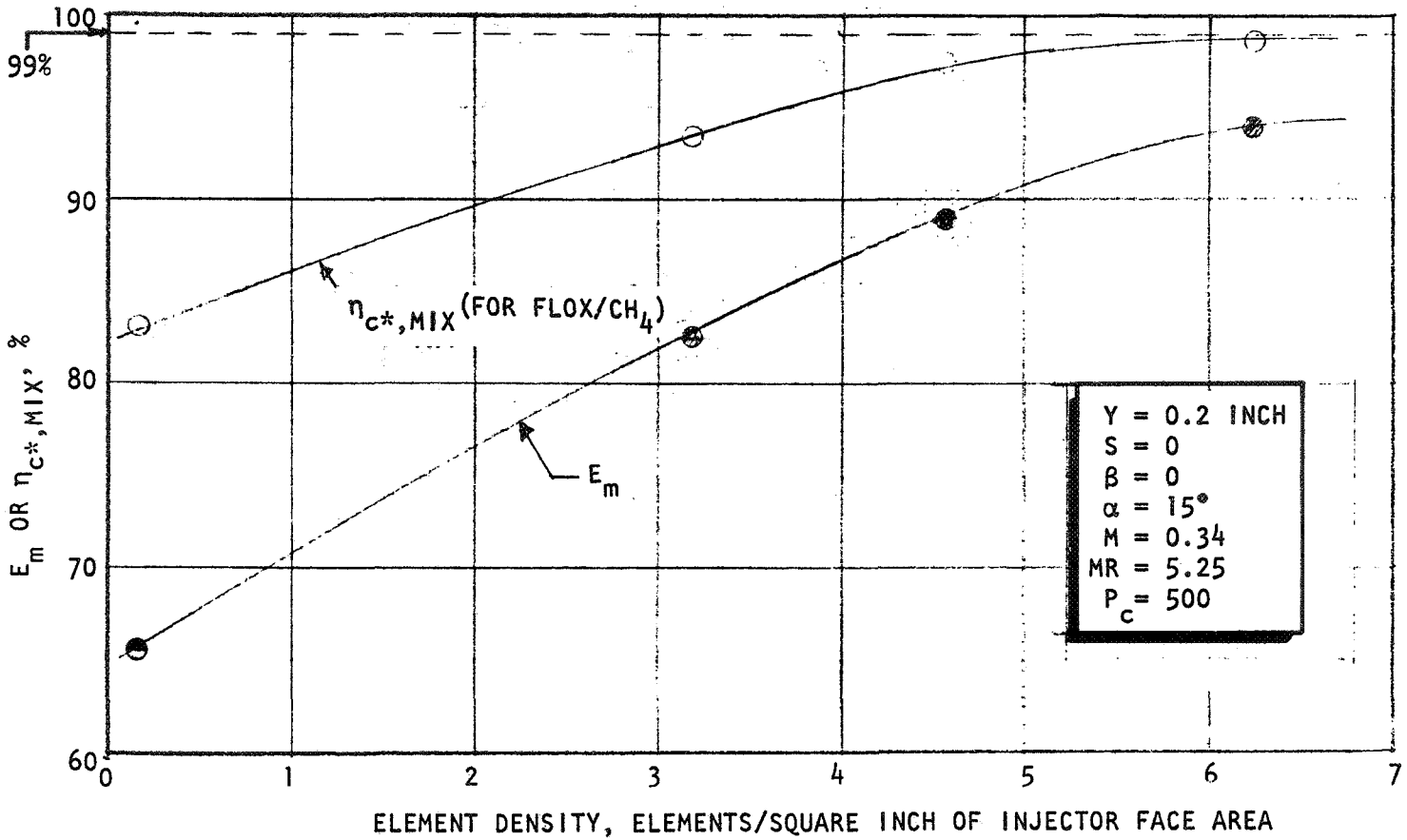

Figure 5. Effect of Element Density on Mixing for Performance Optimized (S = 0; α = 15°) Like-Doublet Injector (Cold-Flow Results)

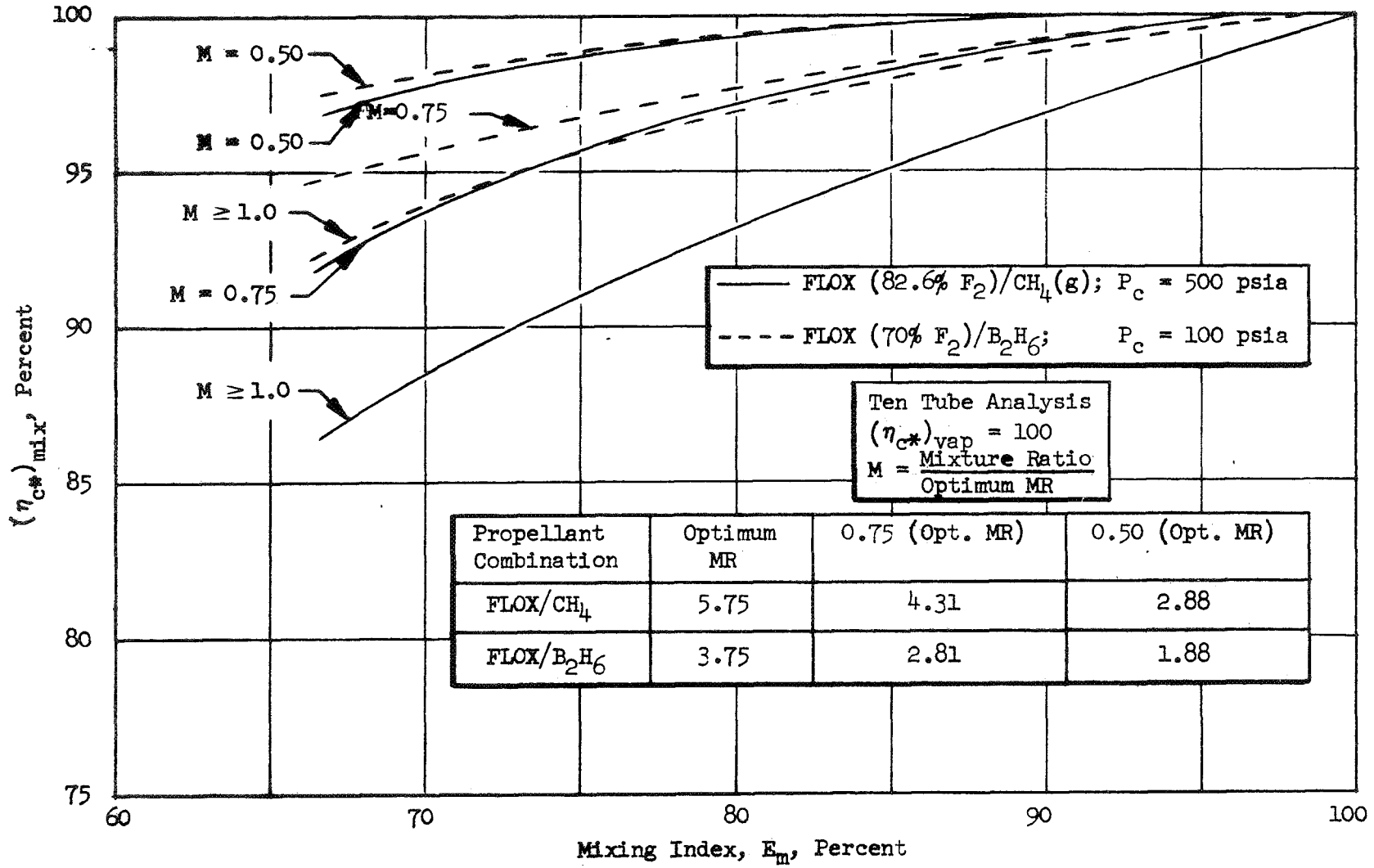

Propellant Combination	Optimum MR	0.75 (Opt. MR)	0.50 (Opt. MR)
FLOX/CH_4	5.75	4.31	2.88
FLOX/B_2H_6	3.75	2.81	1.88

Figure 6. Predicted Effect of Propellant Mixing on Performance for FLOX/CH_4(g) and FLOX/B_2H_6 (Analytical Results)

3.2 COAXIAL ELEMENT PATTERN

Definition of the element configuration, range of experimental data, propellant mixing characteristics, propellant atomization characteristics, and interelement considerations are presented herein for the circular coaxial element pattern.

3.2.1 Element Configuration

A schematic of the high-performance core element configuration which was characterized in this study is presented in Fig. 7 . All the core elements were configured with a diffuser section at the exit of the oxidizer post. The post exit was chamfered at a nominal half-angle of 6 degrees, which is below the value at which separation will occur.

3.2.2 Range of Experimental Data

Cold-flow experiments were conducted with circular coaxial elements (see Fig. 7) over a range of design and operating variables which are directly applicable to the FLOX/light hydrocarbon system. Table II presents the range of variables investigated.

TABLE II. RANGE OF COLD-FLOW VARIABLES FOR CIRCULAR COAXIAL ELEMENT

Parameter	Symbol	Range
Liquid Jet Diameter (oxidizer), inch	D_L	0.070, 0.108, 0.136
Gas Gap Height (fuel), inch	h	$0.005 \leq h \leq 0.041$
Oxidizer Post Recess, inch	R	$0 \leq R \leq 4\ D_L$
Gas Velocity in Annulus (fuel), ft/sec	V_g	$100 \leq V_g \leq 630$
Diffused Liquid Velocity at Post Tip (oxidizer), ft/sec	V_L	$5 \leq V_L \leq 100$
Gas Phase Density, lb/ft^3	ρ_g	$0.3 \leq \rho_g \leq 1.45$
Injected Mixture Ratio	MR	$3 \leq MR \leq 7.5$
Flow Per Element, lb/sec	F	$0.04 \leq F \leq 0.414$

All cold-flow experiments (mixing and atomization) were conducted in pressurized environments to model hot-fire gas-phase densities.

The independent efforts on mixing of the above-listed variables can be found in Ref. 2. However, to present the mixing data in a form convenient for design purposes, the results were correlated as a function of a single parameter.

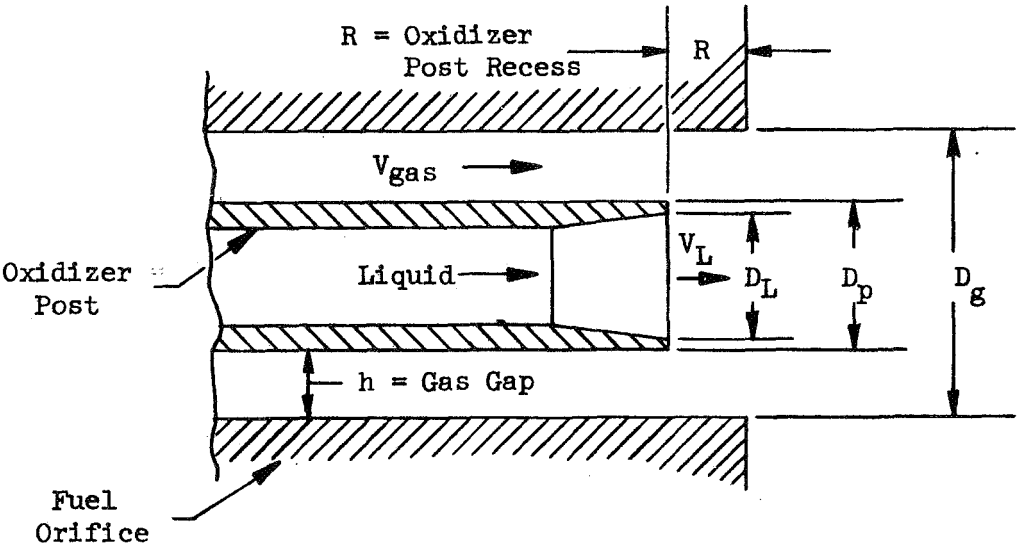

Core Element Configurations (Nominal Dimensions)			
No.	D_L (In.)	D_p (In.)	D_g (In.)
1	0.136	0.146	0.182
2	0.108	0.122	0.166
3	0.070	0.080	0.136

Figure 7. Circular Coaxial Core Element Configurations

3.2.3 Mixing Criteria

The cold-flow mixing results of the program were analyzed to determine if a single parameter could be found to correlate the results in terms of pertinent design and operating variables. The correlating parameter was formulated by considering the dynamic and operating variables which could be expected to control the stripping of the liquid jet by the high-velocity gas annulus. The variables included the kinetic energy of the high-velocity gas ($\rho_g V_g^2$), an operating variable proportional to the residence time of the liquid jet (V_L), the density of the gas phase (ρ_g), and the ratio of liquid mass to gas mass (MR). These variables were formulated into a single parameter by considering the qualitative trends of the data. Figure 8 presents a correlation of the mixing data (E_m) with the parameter $(\rho_g V_g)^2/(MR \cdot V_L)$. As indicated in the figure, the parameter provides a reasonable correlation of the mixing data.

Note that separate curves are necessary for different post recesses (R = 0, $R \approx 1$ D_L). For almost all values of $(\rho_g V_g)^2/(MR \cdot V_L)$, the recessed post gave better mixing, but the difference becomes small for values above about 6000 lbm^2/ft^5-sec.

The data of Fig. 8 can be employed in conjunction with Fig. 6 to determine $\eta_{c^*,\ mix}$ for the FLOX/CH_4(g) propellant combination. For propellant combinations other than FLOX/CH_4(g), Eq. 1 can be employed in conjunction with a multistreamtube analysis to determine $\eta_{c^*,\ mix}$ as a function of E_m.

3.2.4 Atomization Characteristics

Cold-flow atomization tests analogous to the mixing experiments were conducted to define the effects of the design and operating variables listed in Table II. The independent effects of these parameters are tabulated in Ref. 2.

An attempt was made to correlate the atomization data of the program utilizing the parameter $(\rho_g V_g)^2/(MR \cdot V_L)$ which correlated the mixing data (see Fig. 8). However, no reasonable correlation was obtained. The most successful correlation of the atomization data was obtained by replacing the numerator of the mixing correlation parameter by a term proportional to the shear rate at the gas-liquid interface (i.e., $V_g - V_L$). In addition, it can be assumed that the resultant mean drop size will be some fraction of the oxidizer jet diameter. Thus, the resultant mean drop sizes were nondimensionalized by D_L. Figure 9 presents the parameter $\overline{D}/D_L$ as a function of $(V_g - V_L)/V_L \cdot MR)$. As indicated in the figure, the parameters provide reasonable (but certainly not precise) correlations of the atomization data for both flush and recess oxidizer posts.

The data of Fig. 9 can be employed to predict the resulting mass median drop size for an element which operates in a range similar to those employed in this study.

To predict $\eta_{c^*,\ vap}$ for a system $\overline{D}$ and the distribution of the droplets about the median $\overline{D}$ are required as essential input to a computerized vaporization-limited combustion model.

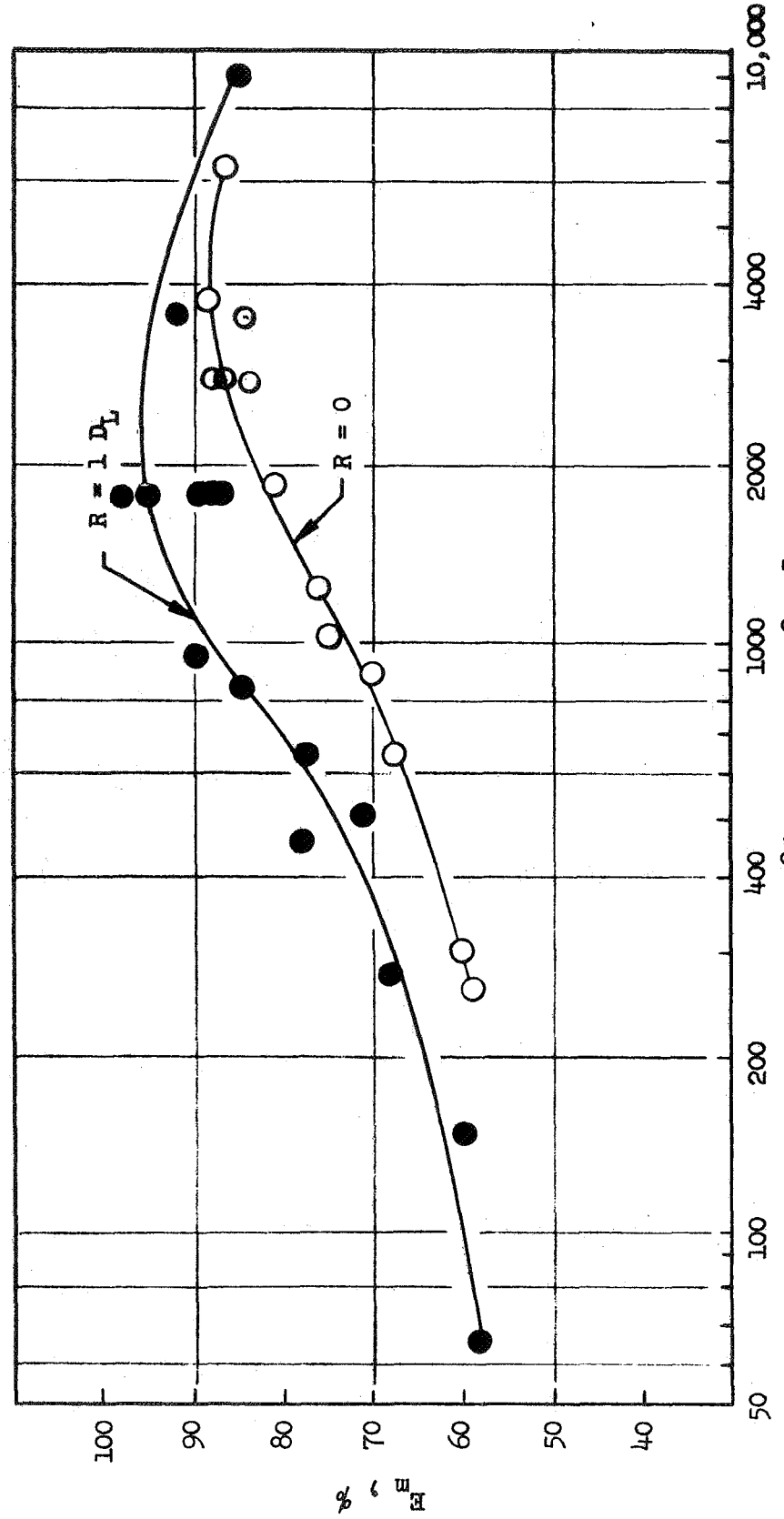

Figure 8. Correlation of Core Element Cold-Flow Mixing Data for Circular Coaxial Element

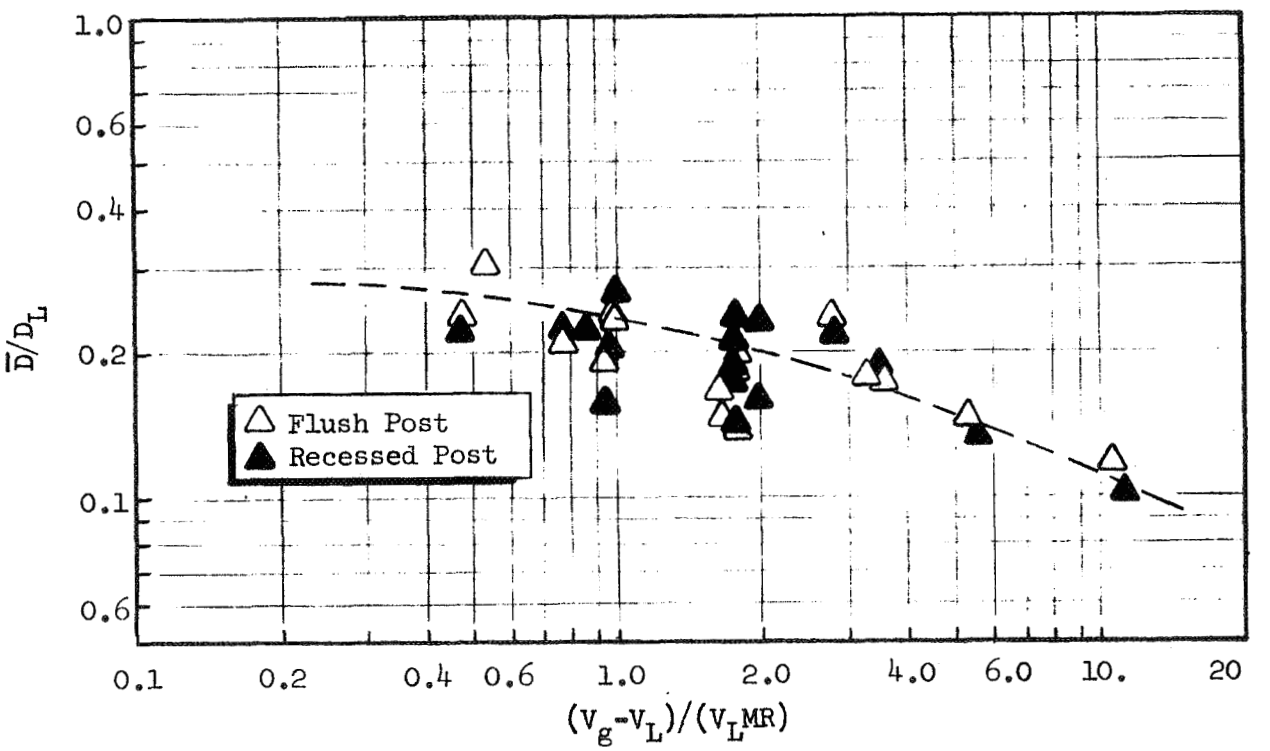

Figure 9. Correlation of Cold-Flow Atomization Data for Circular Coaxial Element

Figure 10 presents normalized drop size distribution data from Ref. 2. Also shown in the figure is the normalized Rosin-Rammler drop size distribution function (Ref. 9). Note the excellent agreement with the coaxial injector data for values of $D/\overline{D}>1.0$. Use of realistic drop size distribution functions for $D/\overline{D}>1.0$ in combustion model programs is critical since these drop size ranges significantly influence the predicted $\eta_{c^*,\ vap}$.

The mass median drop sizes, $\overline{D}$, for a spray sample which conforms to the Rosin-Rammler distribution functions may be converted to an equivalent volume mean drop size by the equation:

$$D_{30} = 0.455\ \overline{D} \tag{5}$$

where

D_{30} = volume mean drop size
$\overline{D}$ = mass median drop size

3.2.5 Interelement Considerations

Since individual element mixing uniformity is quite high for the circular coaxial element, element density effects on mixing are of minor importance for this element type.

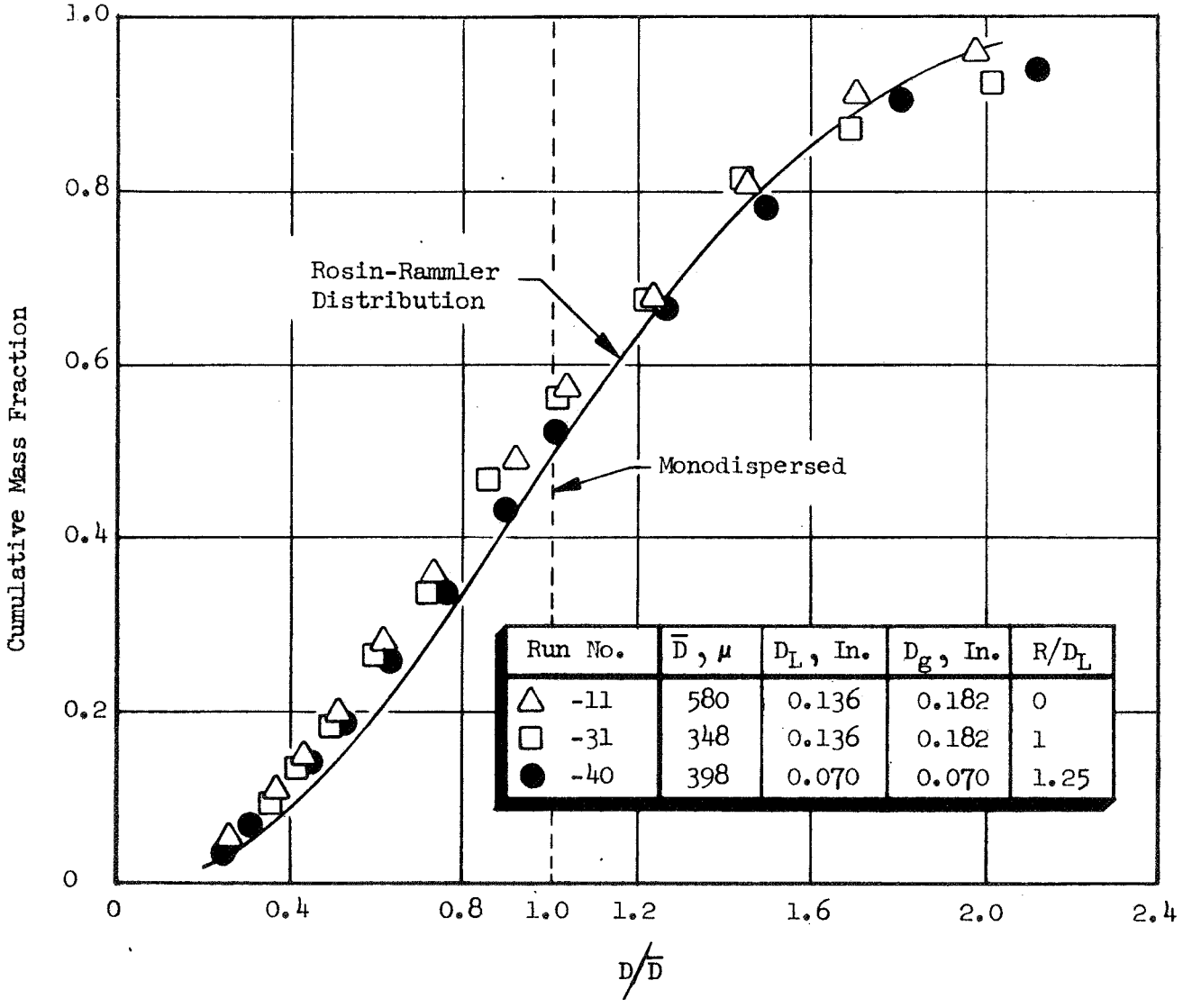

Figure 10. Core-Element Normalized Drop Size Distribution Data for Circular Coaxial Element

4.0 INJECTOR/CHAMBER COMPATIBILITY GUIDELINES

Guidelines for injector element design to achieve chamber compatibility with minimal performance losses due to propellant mass and mixture ratio control (zoning) near the chamber wall are presented herein. Experimental results from both cold-flow mass and mixture ratio distribution and hot-fire tests were used as a basis for the recommended design guidelines. Cold-flow experimental results were used to define element design/operating parameter effects on the resulting gas and liquid mass and mixture ratio distributions. Hot-fire experimental results were employed to define (document) performance losses and chamber heat flux reduction as a function of the pertinent design/operating parameters. Like-doublet and coaxial injector design criteria are presented under separate headings.

4.1 LIKE-DOUBLET PATTERN

Definition of the like-doublet element configurations considered for attainment of chamber compatibility, the range of experimental data, mixing characteristics of the elements tested, and hot-fire verification test results are presented herein.

4.1.1 Element Configuration

Control of chamber wall compatibility with a like-doublet element is attained primarily by intentionally displacing the fans' major axes (i.e., fan spacing $\neq 0$) to provide a mixture ratio bias.

Cold-flow distribution (mixing) tests were conducted with single elements to support design of full-scale hot-fire injectors. The hardware employed was that previously utilized in the performance element studies. These elements were designed to permit testing with fan spacings (S) of 0,0.125, and 0.250 inch.

4.1.2 Range of Experimental Data

The primary test variables were fan spacing (S), fan inclination angle (α), and propellant (oxidizer/fuel) momentum ratio (M). Fan spacings of 0.125 and 0.250 inch were employed. Intra-element spacing (Y) was maintained constant at 0.200 inch. Fan impingement angle (β) was 0 degrees. The fan inclination angle was varied from 0 to 30 degrees at a constant momentum ratio (ℓ/g) of 0.34 and momentum ratio was varied from $\sim$0.34 to 1.2 at a fan inclination angle of 15 degrees for both fan spacings. Fan inclination angles of 0, 15, and 30 degrees were employed. The gas orifice diameter was varied to permit changing the propellant momentum ratio at constant mixture ratio. Mixture ratio was held constant at $\sim$5. The momentum ratio (oxidizer-to-fuel) was varied over a wide range (0.34 to 1.22) by use of a 0.052-inch liquid orifice diameter with gas orifice diameters of 0.055, 0.082, and 0.104 inch. The oxidizer represents the liquid and fuel represents the gas in the discussion that follows.

Data from this test effort were utilized to support design of peripheral element configurations for evaluation in full-scale injectors so that performance losses could be minimized while providing a fuel-rich zone near the chamber wall to reduce chamber heat flux.

4.1.3 Mixing Characteristics

The first topic considered below is the effect of design/operating parameters on performance as influenced by propellant mixing. The fuel (gas) and oxidizer (liquid) flow distribution of single elements, again as a function of design/operating parameters, are then described and flow patterns which would be most desirable for a peripheral injector element are selected.

Performance. Figure 11 presents the results of the experiments to determine the effects of fan inclination on mixing for a momentum ratio (ℓ/g) of 0.34 and fan spacings equal to 0.125 and 0.250 inch. As indicated by Fig. 11, mixing (E_m) is near optimum for a fan inclination angle (α) of approximately 15 degrees for both spacings. As expected, mixing was better with the 0.125-inch spacing than with 0.250 inch between fans.

To determine the effects of propellant momentum ratio upon mixing, the momentum ratio (M_{ox}/M_f) of the elements (S = 0.125 and 0.250 inch) was varied from 0.34 to 1.22 for a constant fan inclination angle of 15 degrees. The results of these experiments are shown in Fig. 12. Mixing levels show a slight decline with increasing M_ℓ/M_g for the 0.250-inch spacing configuration for momentum ratios in excess of about 0.8. For the 0.125-inch spacing configuration, mixing levels were found to increase up to $M_\ell/M_g \cong 0.7$ and, above that value, were found to be nearly constant.

The effect of fan inclination angle on propellant mixing for the performance (S = 0) and chamber-compatible elements are compared in Fig.13 .

Mass and Mixture Ratio Distribution. The same cold-flow data as were used to determine the values of E_m just described were examined to determine potential wall mass and mixture ratio distributions. From a performance standpoint (i.e., maximum E_m) an optimum design for both the 0.250- and 0.125-inch fan spacing configurations would incorporate a fan inclination angle of 15 degrees and a momentum ratio of approximately 0.75. However, as will be discussed in subsequent paragraphs, the optimum performance configurations do not necessarily yield optimum wall mass and mixture ratio distributions.

Figures 14 and 15 present fuel (g) and oxidizer (ℓ) mass flux data for the 0.125- and 0.250-inch spacing configurations, respectively, for a fan inclination angle of 15 degrees and a momentum ratio of approximately 0.75. The scales of the ordinants (liquid and gas mass fluxes) are normalized by a factor of 5; consequently, if the oxidizer value (solid line) and the fuel values (dashed lines) coincide at a point, then the mixture ratio at that point is equal to 5. If the dashed line (fuel) lies about the solid line (oxidizer), then the local mixture ratio is less than 5 (i.e., "low" mixture ratio) and vice versa. The injected mixture ratio was 5.

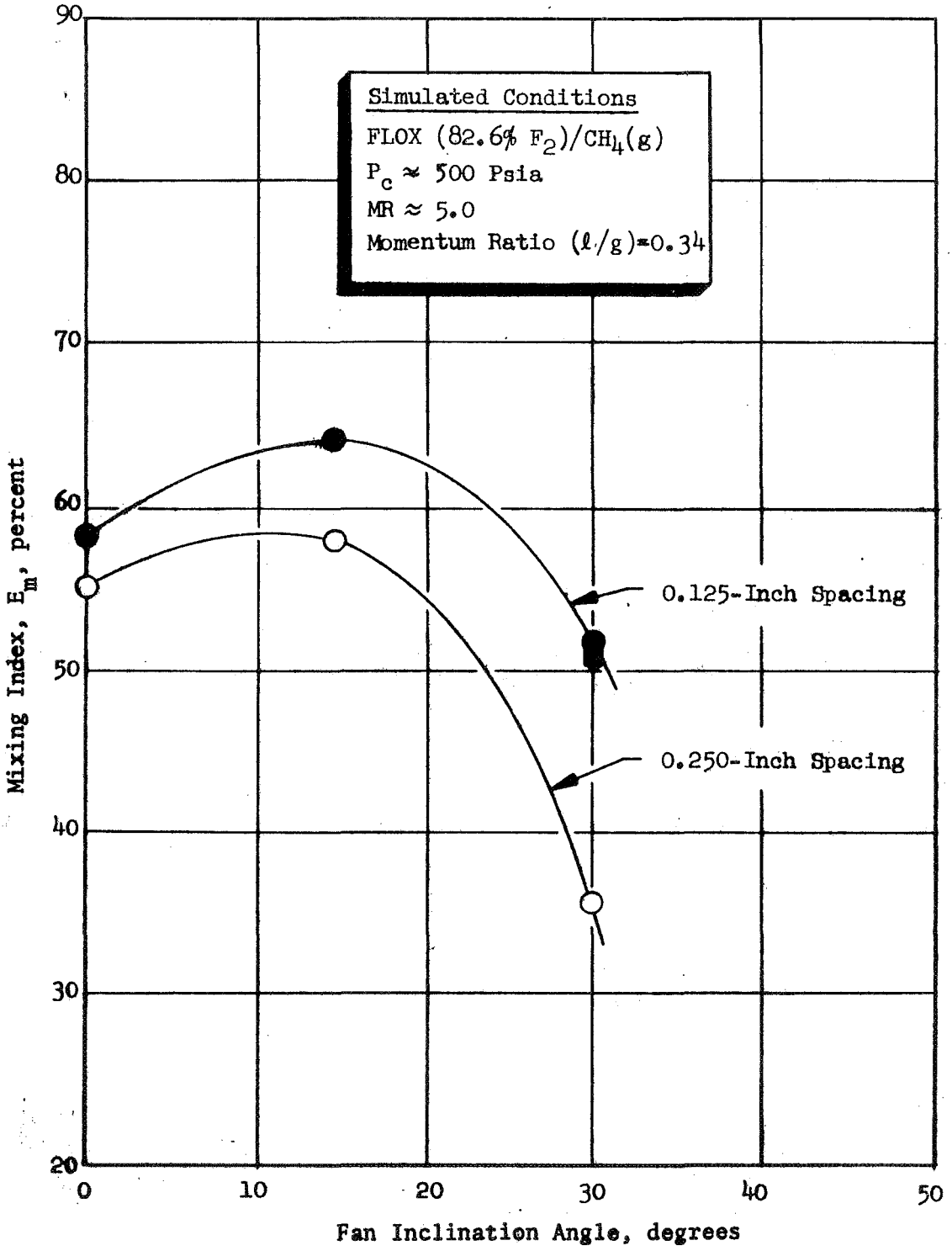

Figure 11. Effect of Fan Spacing and Inclination Angle on the Mixing Index E_m for Chamber Compatible Single-Element Gas/Liquid Like-Doublet Elements

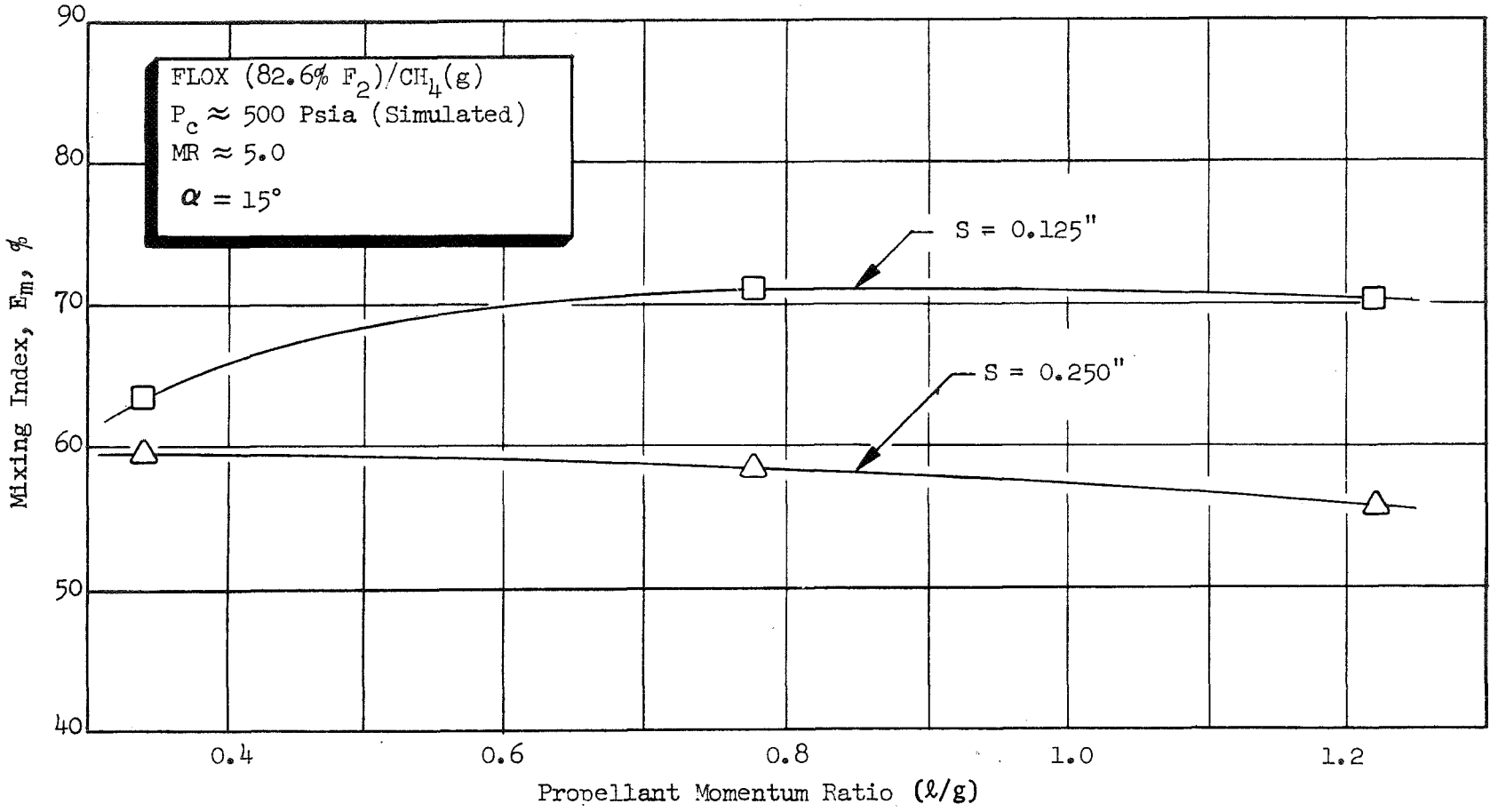

Figure 12. Effect of Oxidizer to Fuel Momentum Ratio on E_m for Single-Element Chamber Compatible Gas/Liquid Like-Doublet Elements (Cold-Flow Results)

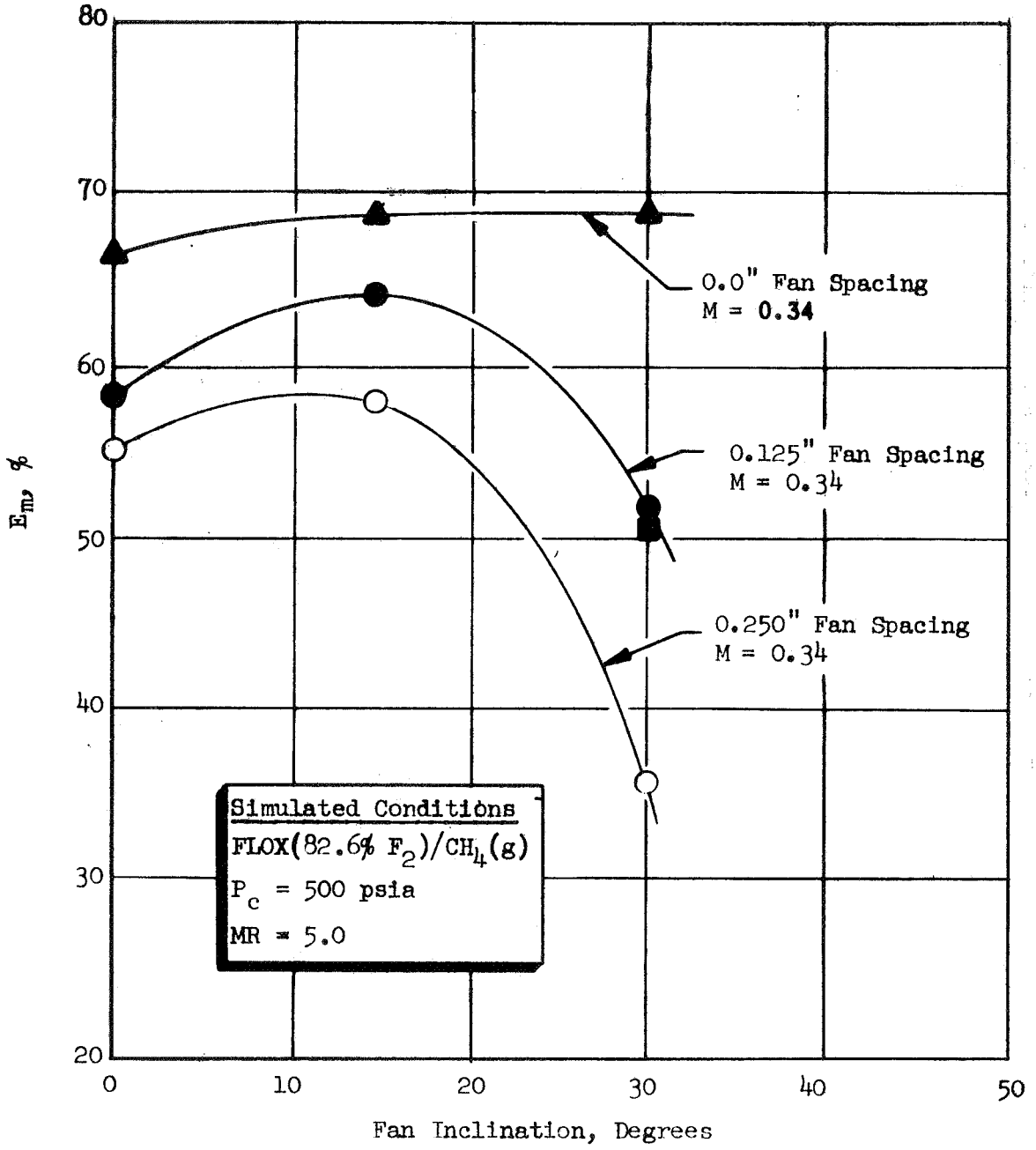

Figure 13. Effect of Fan Spacing and Inclination Angle on the Mixing Index, E_m, for Single-Element Gas/Liquid Like-Doublet Elements

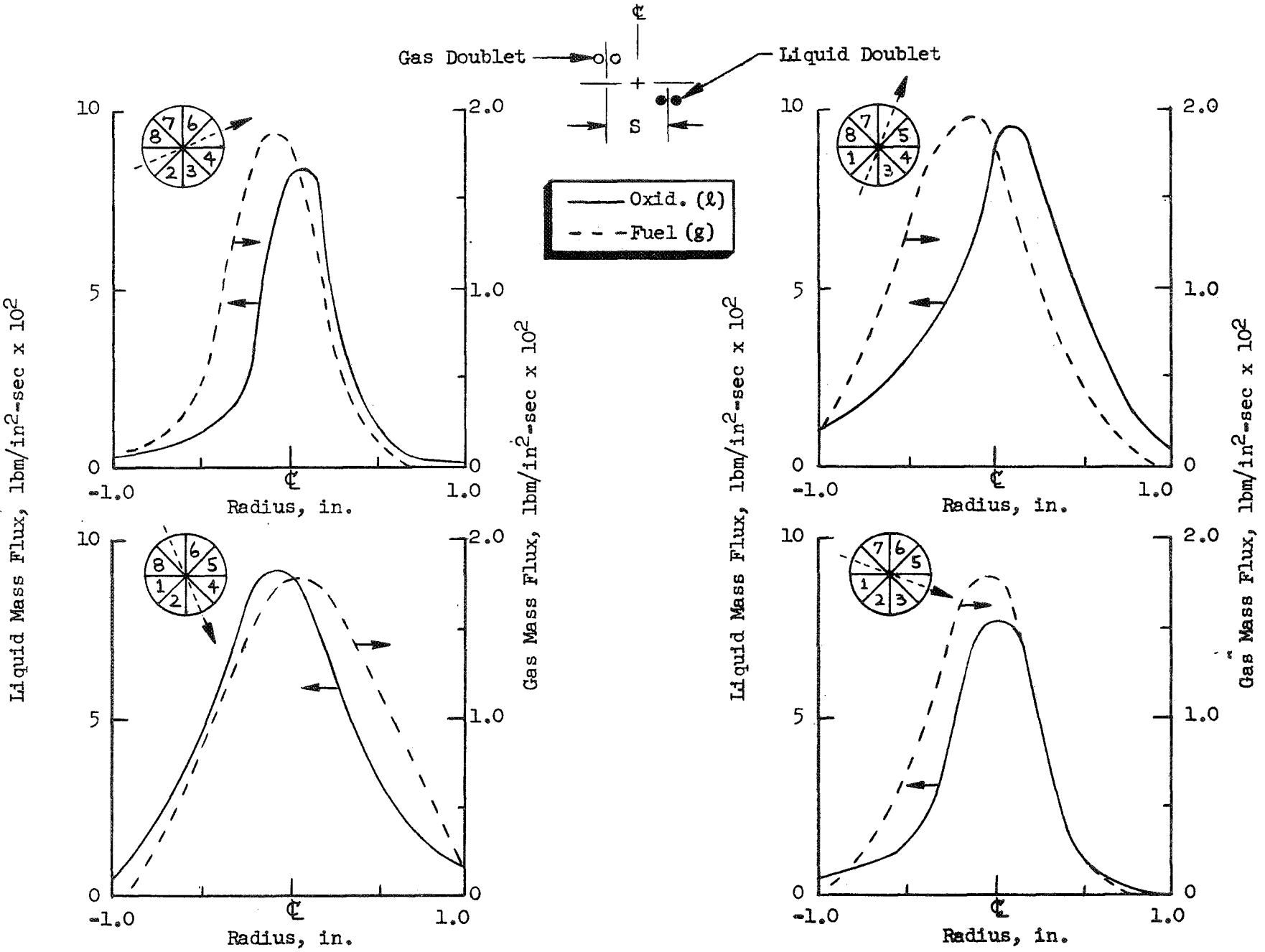

Figure 14. Fuel and Oxidizer Mass Flux Data for Momentum Ratio (o/f) = 0.775, α = 15 Degrees, S = 125-Inch Test

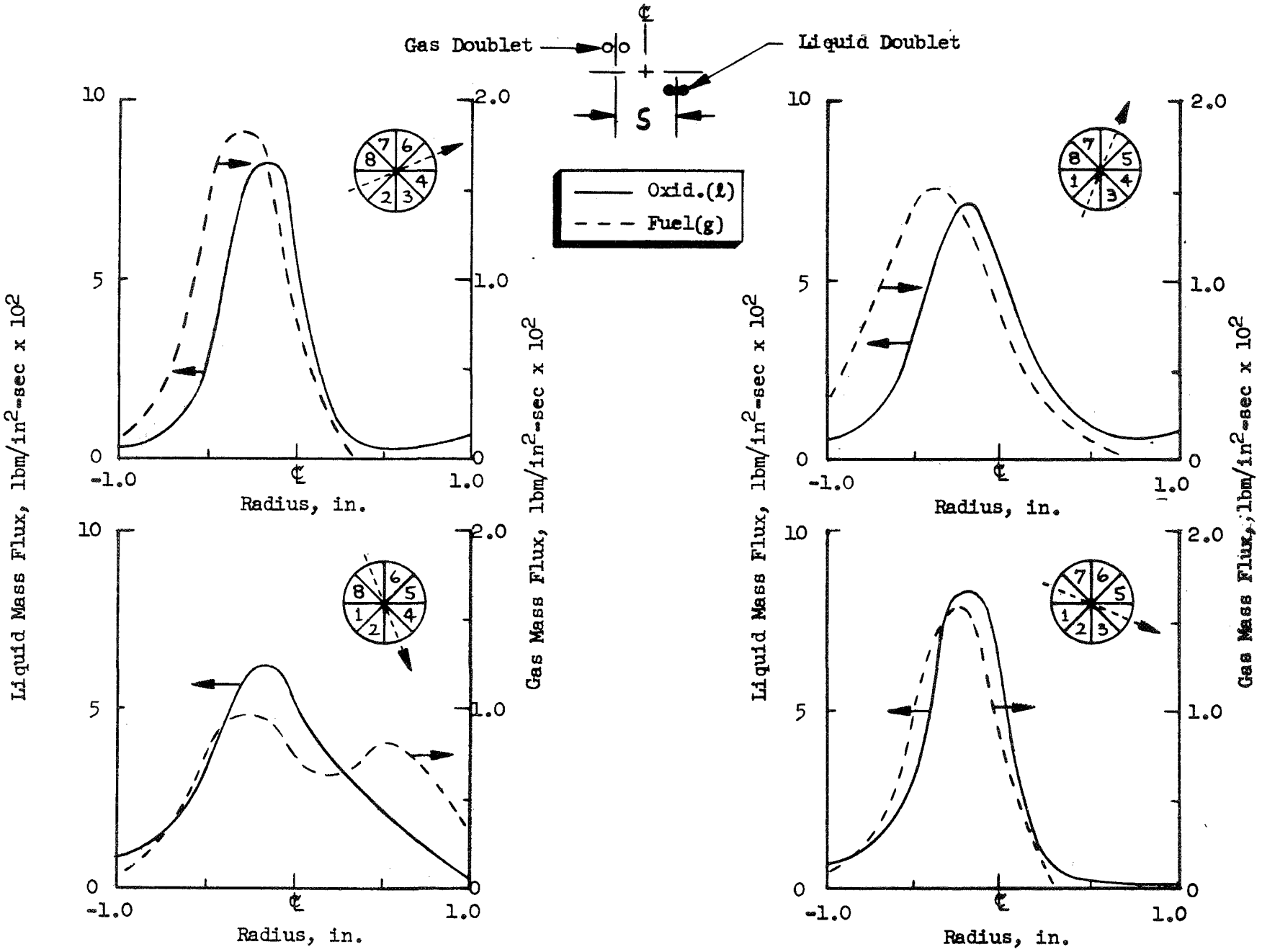

Figure 15. Fuel and Oxidizer Mass Flux Data for Momentum Ratio (o/f) = 0.775, α = 15 Degrees, S = 0.250-Inch Test

Also illustrated on each plot is the angular orientation of that profile with respect to the element orientation.

Examination of Fig. 14 for the 0.125-inch configuration (S = 0.125 inch) with α = 15 degrees and M_{ox}/M_f = 0.775, shows a relatively low mixture ratio (MR<5) region exists in adjacent sectors 8, 1, and 2 so this would be the most desirable zone to have near the wall (for this configuration). Examination of Fig. 15, obtained from a 0.250-inch spacing configuration with α = 15 degrees, M_{ox}/M_f = 0.775 shows that a low mixture ratio periphery (MR<5) would be possible if the wall were to be placed adjacent to sectors 1 and 2. However, examination of all the data with M_{ox}/M_f = 0.34 (S = 0.125, 0.250 inch, α = 0, 15, 30 degrees) revealed that the configuration of α = 0 degrees and S = 0.250 inch resulted in the lowest potential wall mixture ratio. These data are shown in Fig. 16. Note that a strong, low mixture ratio bias would be obtained if the chamber wall were placed adjacent to either section 1, 8, or 7. The absolute values of gas mass flux in these sectors are substantially higher than the best sectors shown in Fig. 14 and 15 (α = 15 degrees, M_{ox}/M_f = 0.775, S = 1.25 and 0.250 inch).

Selection of α = 0 degrees, S = 0.250 inch instead of α = 15 degrees, S = 0.250 inch would result in a maximum loss (assuming no interelement mixing effect) in mixing performance (corresponding to the decrease in E_m) of approximately 3 percent. However, considering the mass and mixture ratio profiles of the α = 0 degrees, S = 0.250-inch case as opposed to α = 15 degrees, S = 0.125 or 0.250 inch, the former is clearly superior from the standpoint of providing wall mixture ratio bias.

Examination of the mass and mixture ratio profiles for the tests to define the effects of propellant momentum revealed (E_m data shown in Fig. 12 that the propellant momentum ratio did not have a significant effect on the wall mass and mixture ratio distributions. Thus, a value of 0.75 for the element momentum ratio should provide near-optimum performance (E_m) while providing a "low" mixture ratio wall region.

Based on these cold-flow data, the following element design parameters are recommended for 0.125 and 0.250-inch fan spacing injector configurations: fan spacing, S = 0.125 inch; fan impingement angle, β = 0 degrees; intra-element spacing, Y = 0.20 inch; fan inclination angle, α = 15 degrees; momentum ratio (ox/fuel) = 0.75; fan spacing, S = 0.250 inch; fan impingement angle, β = 0 degrees, intra-element spacing, Y = 0.20 inch; fan inclination angle, α = 0 degrees; momentum ratio (o/f) = 0.75. Based on the data in Fig. 14 and 16, the elements should be aligned with sectors 1 (S = 0.125 inch) and 8 (S = 0.250 inch) adjacent to the chamber wall.

Basically, the 0.250-inch fan spacing design represents the configuration indicated by cold-flow data to offer the best chamber compatibility, though at some cost in performance. The recommended 0.125-inch fan spacing design concept results from a compromise between mixture ratio control and performance potential in which performance should remain relatively high, but wall protection is still provided. Only the 0.250-inch fan spacing design was fabricated and hot-fire tested.

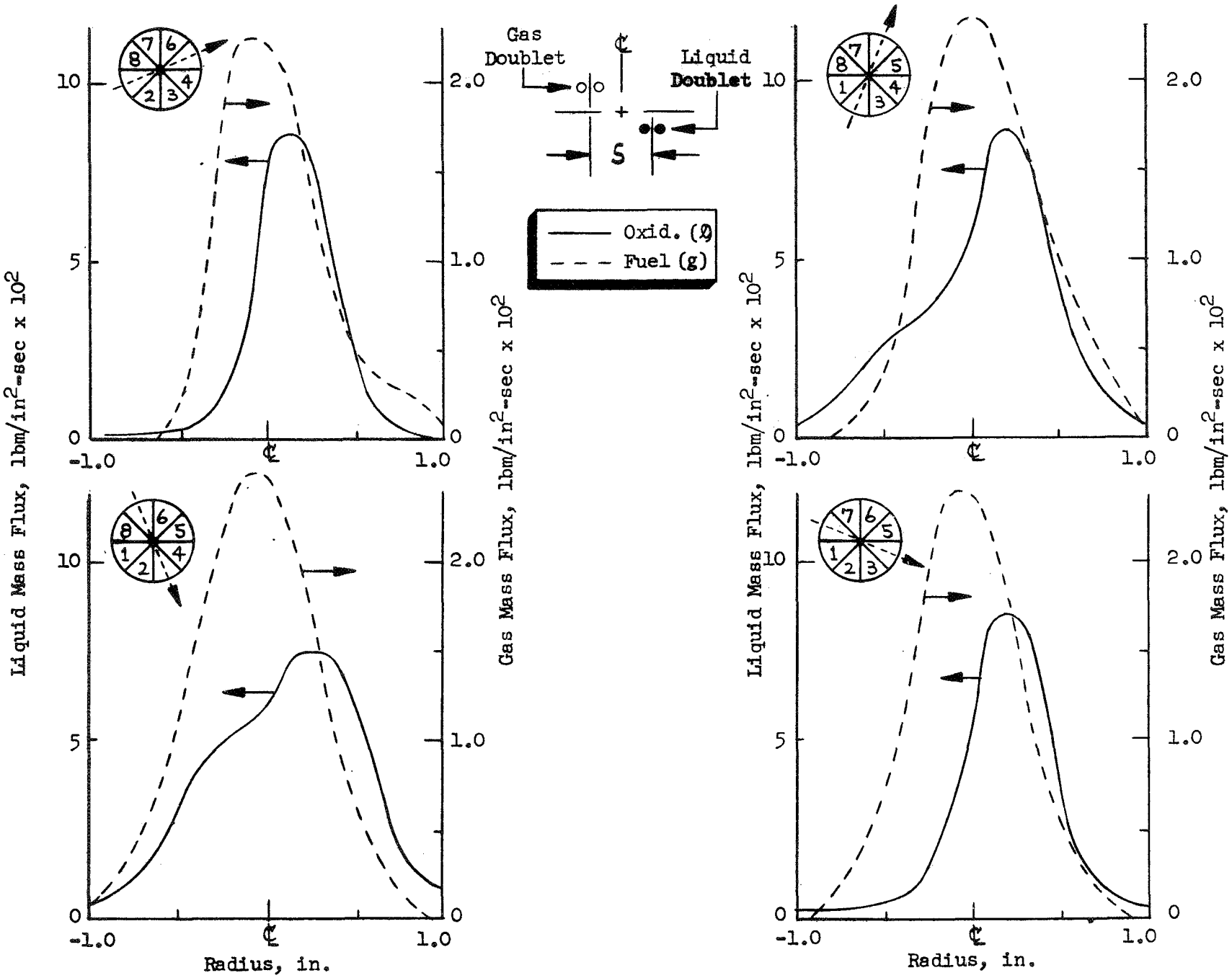

Figure 16. Fuel and Oxidizer Mass Flux Data for Momentum Ratio (o/f) = 0.34, α = 0 Degrees, S = 0.250-Inch Test

4.1.4 Chamber Heat Transfer Characteristics

The effects of element fan spacing, orientation of the element with respect to the chamber wall, and operating conditions (chamber pressure, mixture ratio, and peripheral zone mass flow) on chamber wall heat flux are presented here for the like-doublet element pattern.

Three full-scale injectors were hot-fire evaluated. One (injector A) contained 37 high-performance (S = 0) elements. The fuel doublets were on the chamber wall side of the element and the spray fans were essentially perpendicular to the chamber wall. The second (injector C) contained 35 chamber-compatible elements (S = 0.250 inch; α = 0). The fuel doublets were again on the chamber wall side of the element. However, in this case, the elements had their fans more nearly parallel to the chamber wall. Based on the single-element cold-flow data, the peripheral zone elements were turned slightly ($\sim$20 degrees) from parallel to the wall to provide the lowest possible mixture ratio region adjacent to the wall. The third injector (injector D) was an optimized configuration with separately manifolded "high-performance" core and "chamber-compatible" peripheral zones. The core elements were similar to those of the A injector, while the peripheral zone elements were similar to those of the C injector. The elements were 3/4-scale reductions of those in the A/C injectors. Therefore, fan spacing for the peripheral elements was 3/16 inch. This injector contained 63 elements arranged in four rings. The inner three rings (42 elements) constituted the core region and the outer ring (21 elements) was the peripheral zone.

Performance of the three injectors at design operating conditions (P_c = 500 psia; MR = 5.25) was:

Injector Configuration	η_{c^*}, %
A	96.5
C	92.5
D	97.5

Schematic representations of the A, C, and D injectors are presented in Fig. 17, 18, and 19, respectively.

Chamber heat transfer characteristics for the high-performance (A) and chamber-compatible (C) injectors are presented in Fig. 20 and 21. The effect of injector design and chamber pressure on chamber heat flux is presented in Fig. 20. Chamber heat flux is shown plotted as a function of the axial distance from the injector for both injectors. The chamber contour (L* = 40 in.; ε_c = 3) also is illustrated. Results are presented for chamber pressures of 500 and 250 psia at a mixture ratio of 5.5. Nominal design operating conditions are a chamber pressure of 500 psia and overall mixture ratio of 5.25. The effect of injector design on chamber heat flux is readily apparent. In general, local heat fluxes for the C injector (fan spacing = 1/4 inch), which was designed for chamber compatibility, are approximately half those of the high-performance A injector (fan spacing = 0) throughout the chamber. Even in the nozzle throat region,

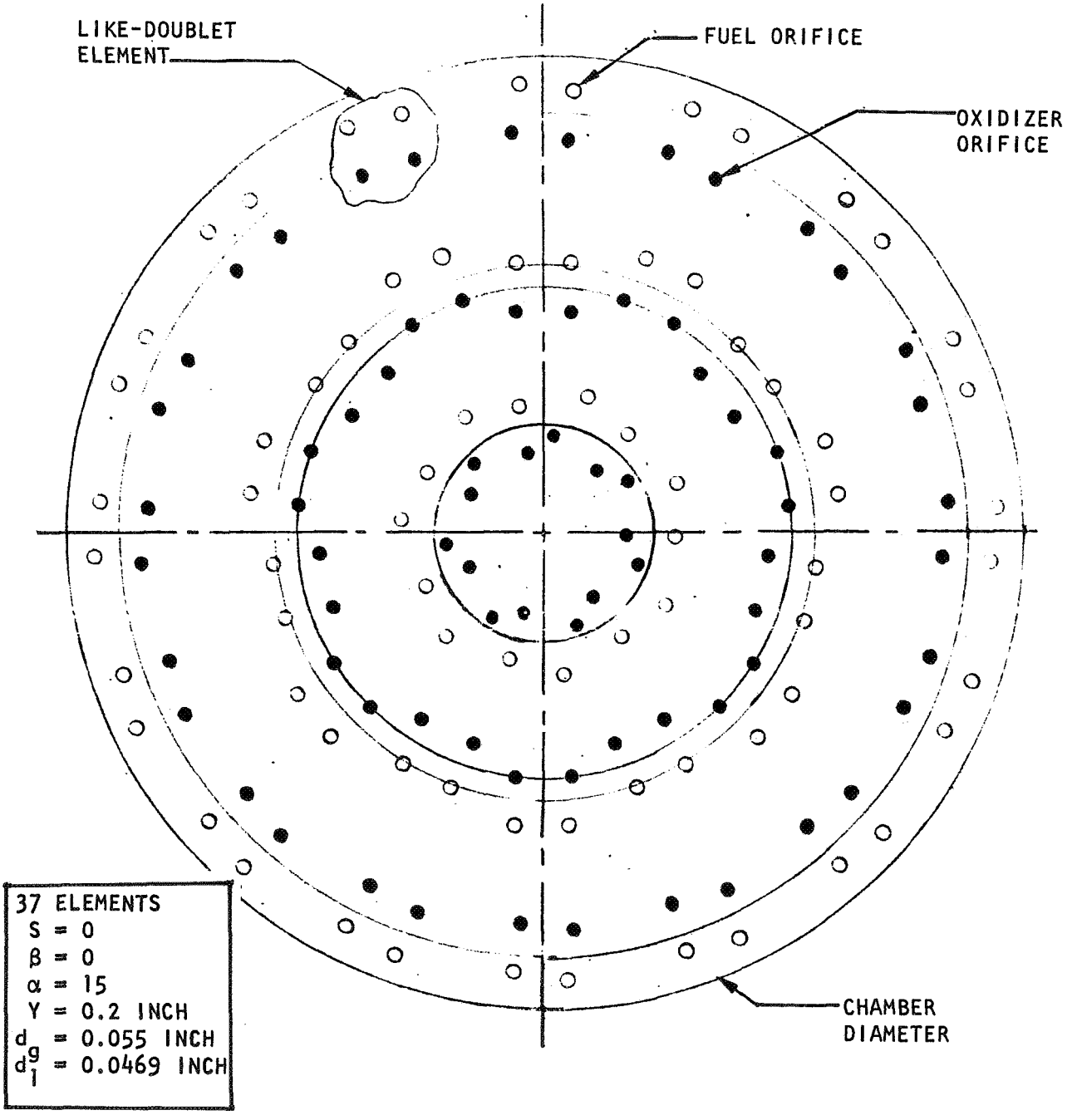

Figure 17. Schematic Representation of Face Pattern of Injector A

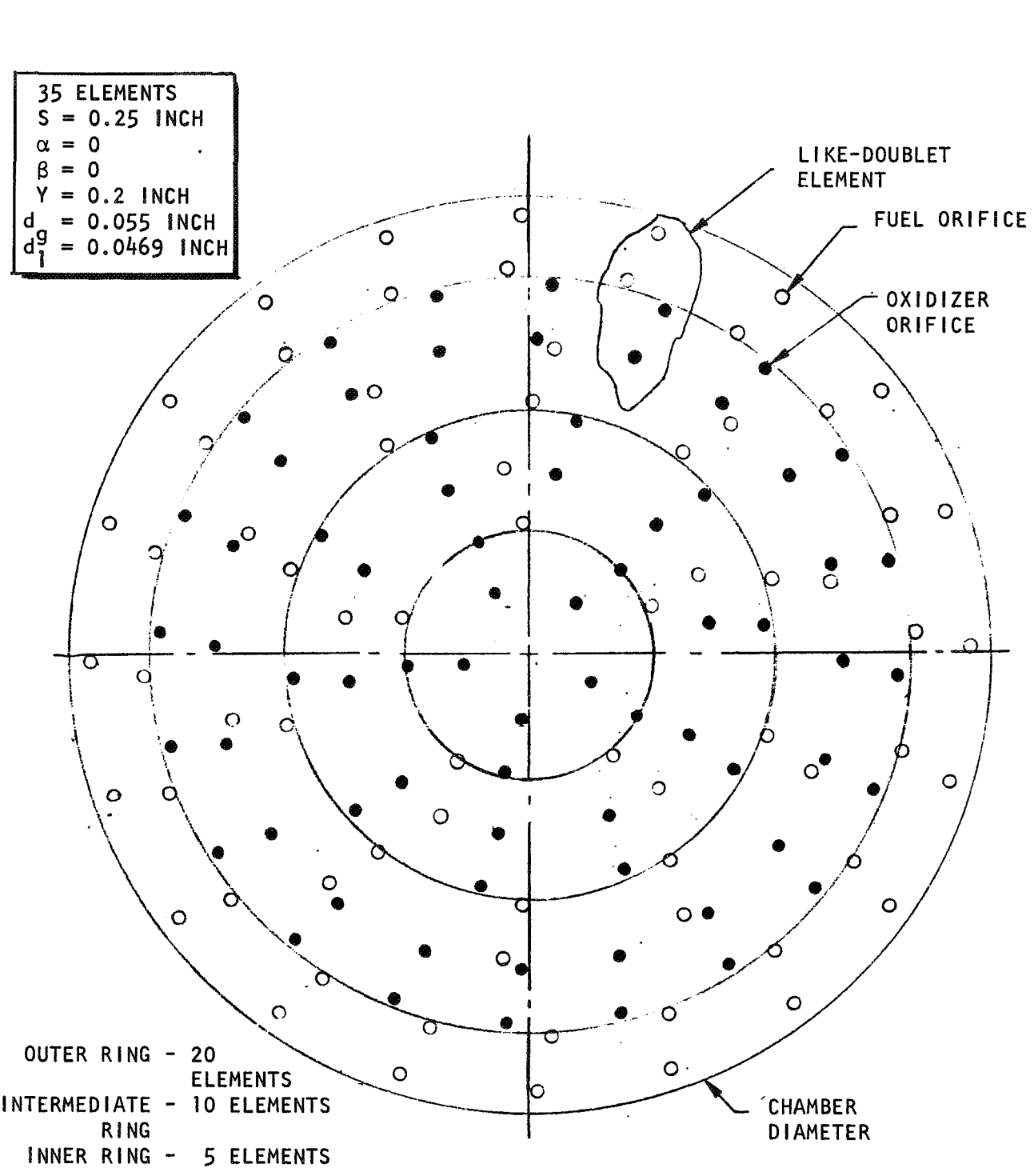

Figure 18. Schematic Representation of Face Pattern of Chamber-Compatible C Injector

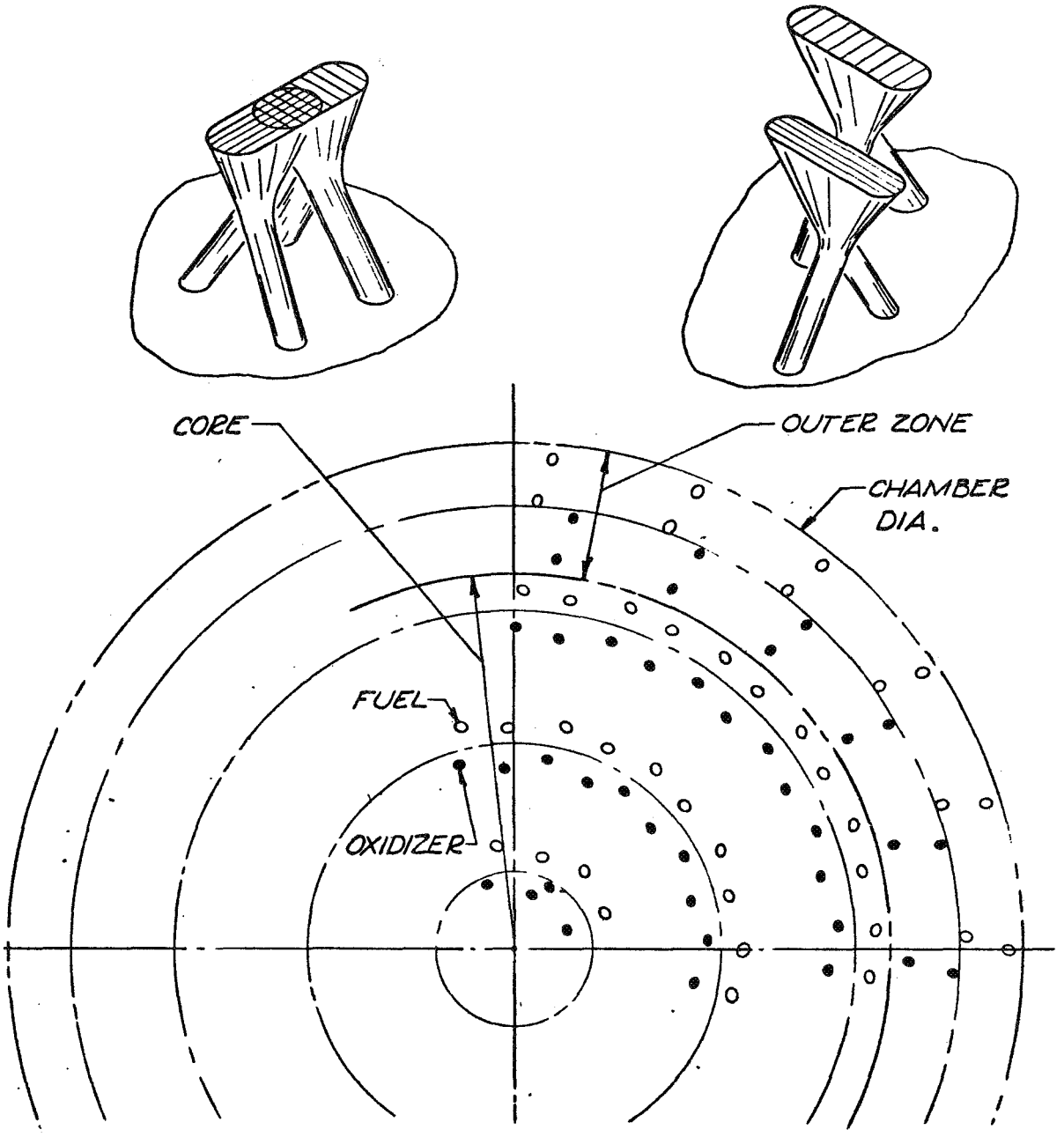

Figure 19. Illustration of Face Pattern and Element Fan Alignment for Optimized Like-Doublet Injector (Injector D)

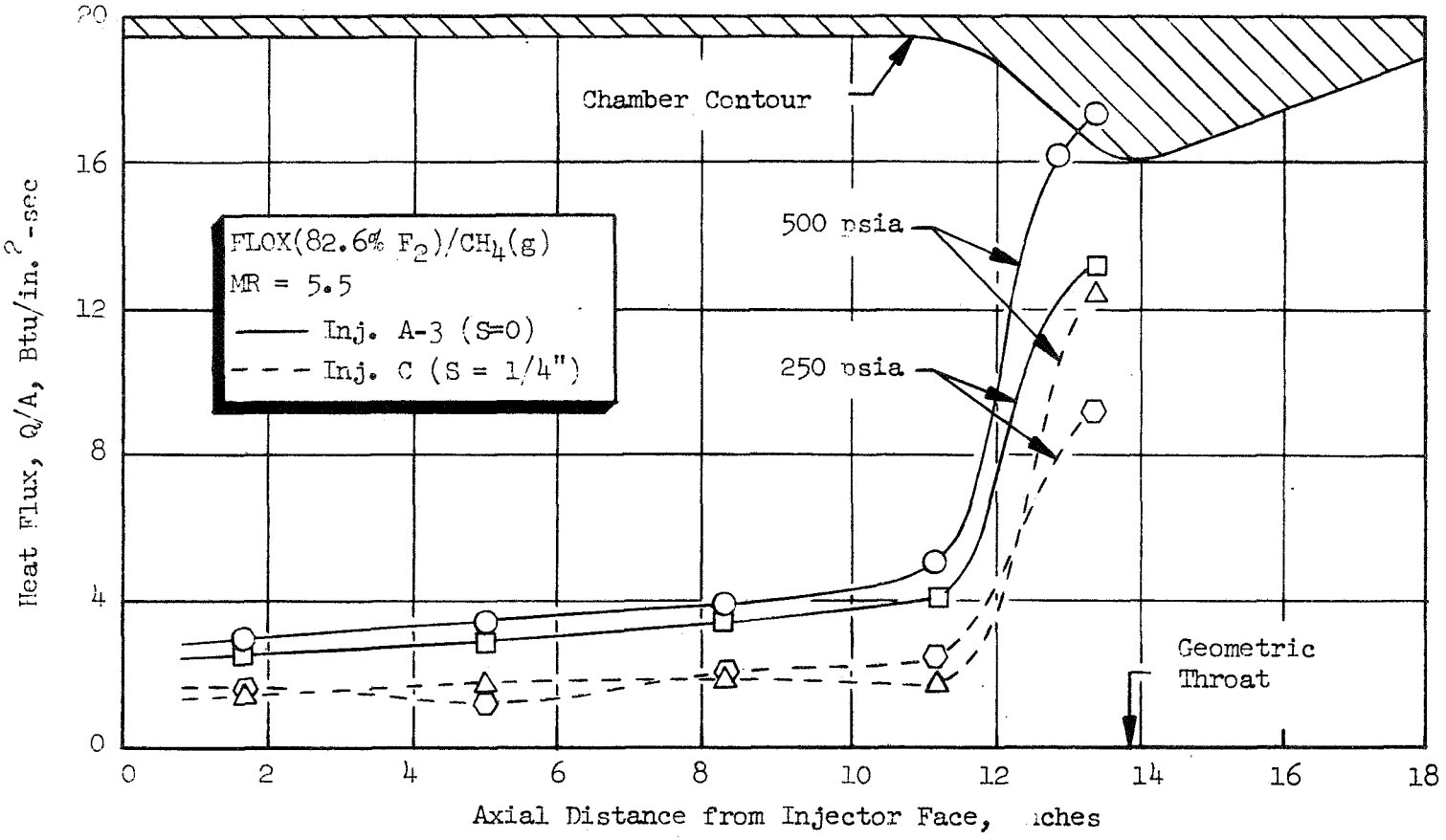

Figure 20. Effect of Injector Design and Chamber Pressure on Thrust Chamber Heat Transfer Characteristics

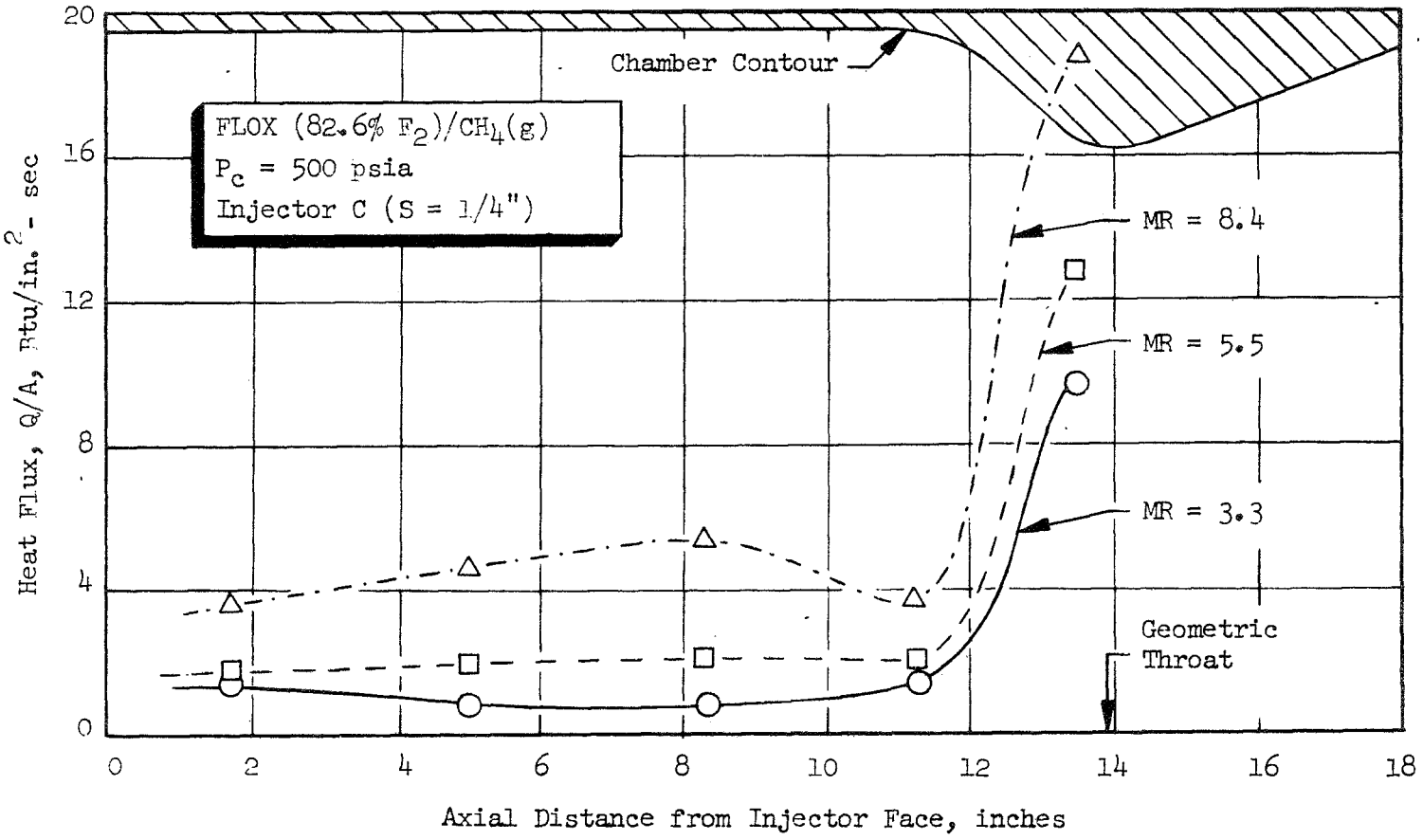

Figure 21. Effect of Mixture Ratio on Thrust Chamber Heat Transfer for Chamber Compatible C Injector

heat flux with the C injector is only about 70 percent of that with the A injector at similar operating conditions. Chamber heat fluxes for the two injector configurations appear to increase only slightly with chamber pressure variations between 250 and 500 psia. In the nozzle region, heat flux is proportional to chamber pressure to approximately the 0.8 power for each injector, as would be predicted from standard heat transfer equations (pipe flow, turbulent boundary layer regime).

The effect of mixture ratio on chamber heat transfer characteristics is shown in Fig. 21 for the C injector configuration. Local heat flux is plotted as a function of axial distance from the injector for three tests conducted at a chamber pressure of 500 psia and mixture ratios of 3.3, 5.5, and 8.4. As noted, chamber and nozzle heat flux increases significantly with increasing mixture ratio.

The effects of peripheral zone element design, mixture ratio, and percent mass flow to the peripheral zone on the average chamber heat flux is summarized in Fig. 22 for all three injectors. These data show that chamber wall heat flux can be significantly reduced by proper design of the peripheral elements to control the peripheral zone mixture ratio and/or the percentage of mass flow to the periphery.

4.2 COAXIAL CONFIGURATION

Definition of the coaxial element configurations considered for chamber compatibility, the range of supporting experimental data, mixing characteristics of the elements tested, and hot-fire verification results are presented herein.

4.2.1 Element Configurations

In this study, two coaxial-type elements were characterized for chamber wall compatibility. Schematics of the two configurations along with their respective dimensions are shown in Fig. 23.

A baseline configuration was chosen which consisted of a "core"-type element with an adjacent boundary layer coolant (BLC) hole. The second peripheral element configuration consisted of the scarfed post with oxidizer jet swirl. The scarfed post with swirl element was designed with a nominal post scarf angle of 22-1/2 degrees, as shown in Fig. 23. The oxidizer jet was swirled by employing an in-line helical with a nominal helix angle of 45 degrees.

4.2.2 Range of Experimental Data

The percent of fuel used as film coolant was varied from 0 to 10 percent* using the BLC concept. Test conditions simulated were an overall mixture ratio of 5.25 and chamber pressure of 500 psia. Both single-element hot-fire and cold-flow tests were conducted.

4.2.3 Mixing Characteristics

Performance Characteristics. Mixing experiments conducted with the two configurations shown in Fig. 24 indicated that mixing performance of the two are nearly

*Defined as percent of total *fuel* flow.

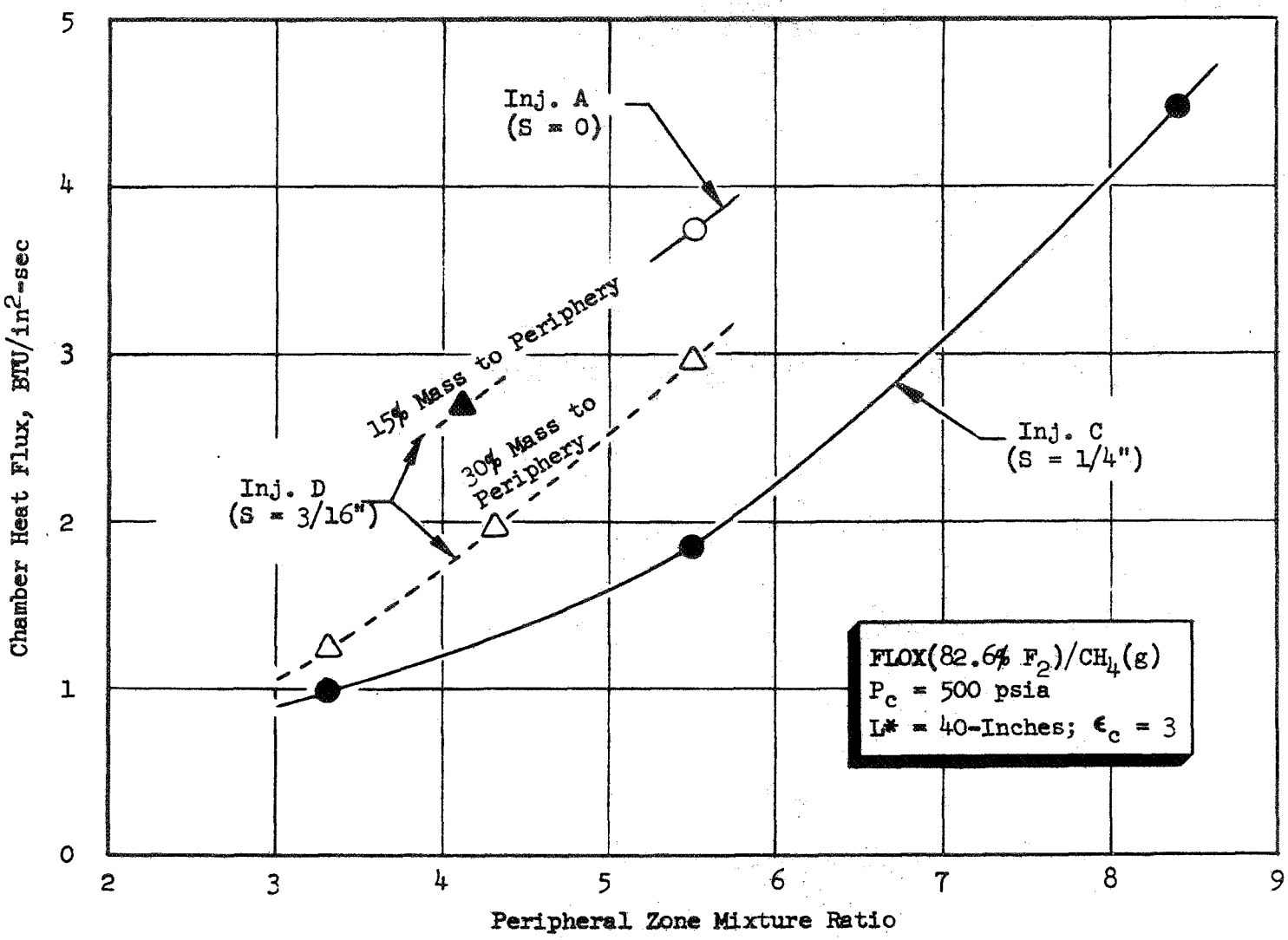

Figure 22. Effect of Peripheral Zone Element Design, Mixture Ratio, and Percent Mass Flow on Average Cylindrical Chamber Heat Flux for FLOX/CH_4(g) Like-Doublet Injector

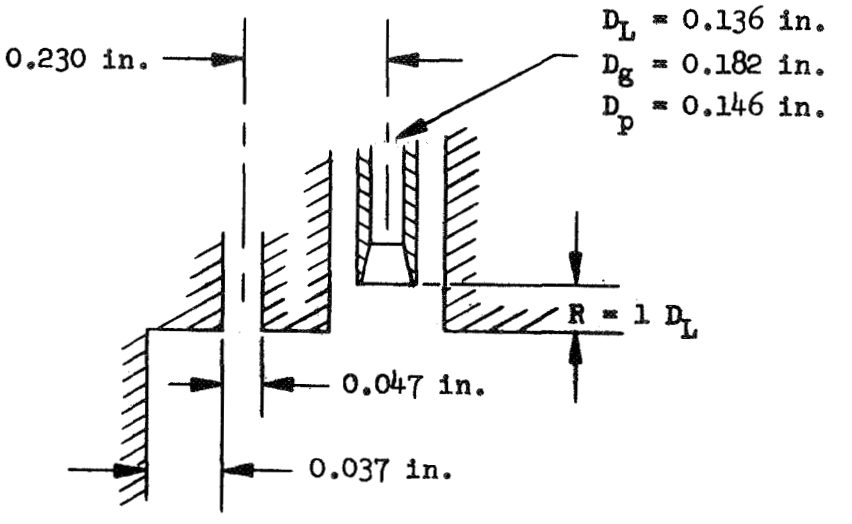

BLC Concept

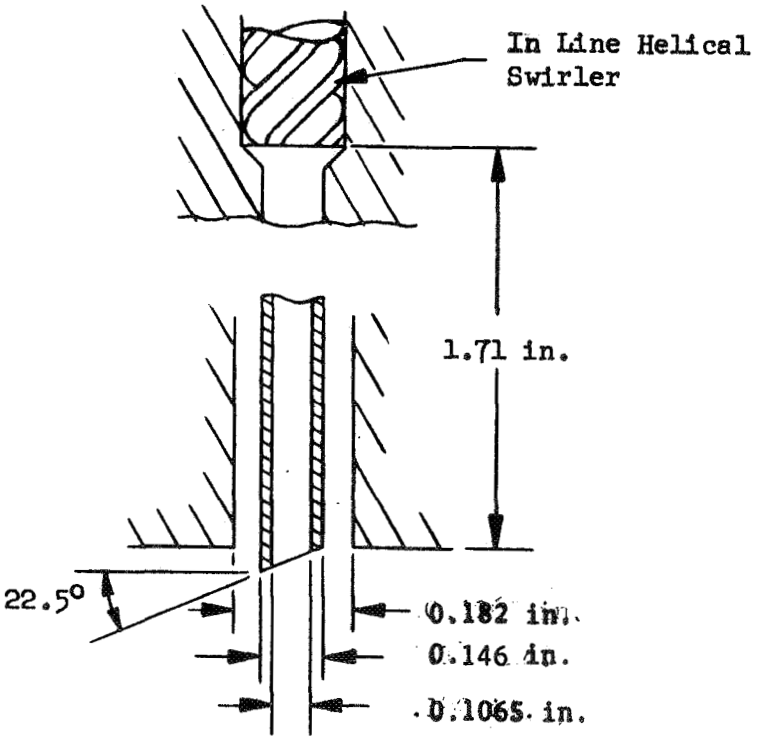

Scarfed Post With Swirl Concept

Figure 23. Circular Coaxial Peripheral Element Configurations

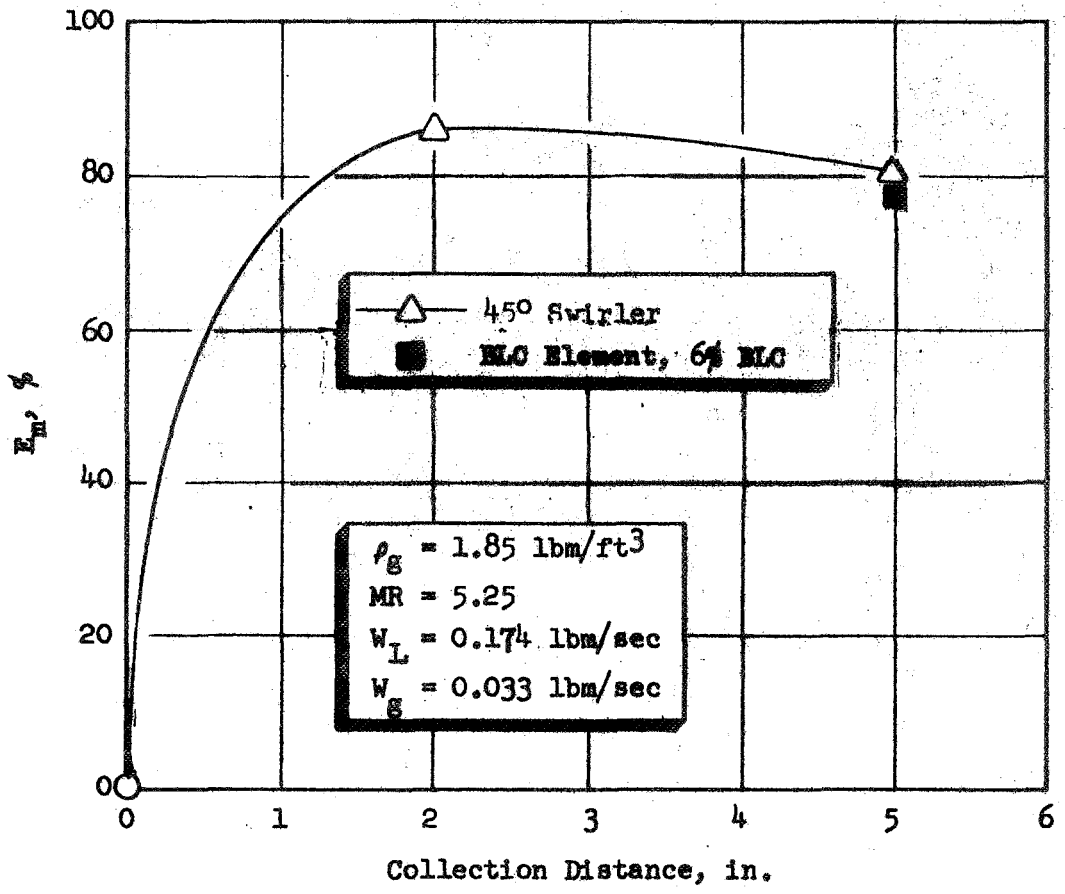

Figure 24. Mixing Performance of Scarfed Post With Swirler Configuration and BLC Element

equivalent. Figure 24 presents mixing level, E_m, as a function of distance from the injector face for the two configurations.

Extensive atomization data for the two configurations are not available. For the operating conditions shown in Fig. 24 , the respective mass median drop sizes are 580 and 590 microns for the BLC and scarfed post configurations.

Mass Flux Profiles. Since chamber wall heat flux is primarily a function of wall zone mass and mixture ratio, the results of the mixing tests provide information in regard to the mass flow characteristics of the elements. Figure 25 presents "normalized" mass flux profiles for both configurations. Note that the mass flux is "normalized" only with respect to total propellant flowrate and not with respect to area.

Plotting the "normalized" mass fluxes allows for a visual determination of the uniformity of the spray field. That is, if local values for the "normalized" liquid and gas mass flux coincide then, at that point, the local mixture ratio is equal to injected mixture ratio. If the liquid values are higher than the gas, then the local mixture ratio is greater than the injected mixture ratio, and vice versa. For complete mixing (i.e., E_m = 100%) the curves would coincide both spacially and in magnitude.

Figure 25 presents normalized mass flux data for both the scarfed post and BLC configurations with $\dot{w}_{BLC}$ = 0.006 lbm/sec. The data are plotted for the hypothetical wall region of interest (Sectors 2 and 3). Examination of the cold-flow data shows that both configurations possess characteristics which could provide enhanced injector/chamber compatibility. The flux profiles for the scarfed post with swirl show that the element displaces mass away from the wall region, but the local wall mixture ratios are higher than the injected mixture ratios. That is, near the wall, local values of "normalized" liquid mass flux are higher than gas mass flux.

The flux profiles for the BLC tests show that liquid distribution is not affected by the showerhead BLC flow. However, the displacement of the gas distribution from the centerline of the element is evident. The resulting BLC element flow field is characterized by a low wall region mixture ratio, but with relatively small increase in mass flux near the wall.

The relative merits of each configuration as a peripheral element were investigated with single-element hot firings. These data showed the relative merits of low wall mixture ratio versus low wall mass flux.

4.2.4 Chamber Heat Transfer Characteristics

Chamber Wall Heat Flux - Single Element. Heat flux data for the scarfed post with swirl and the BLC peripheral element data are shown together in Fig. 26 . Even at the 6.8% BLC level, wall heat flux levels are lower (~10%) than those obtained with the scarfed post with swirl element. This is true in spite of the fact that the performance levels are significantly higher with the BLC configuration.

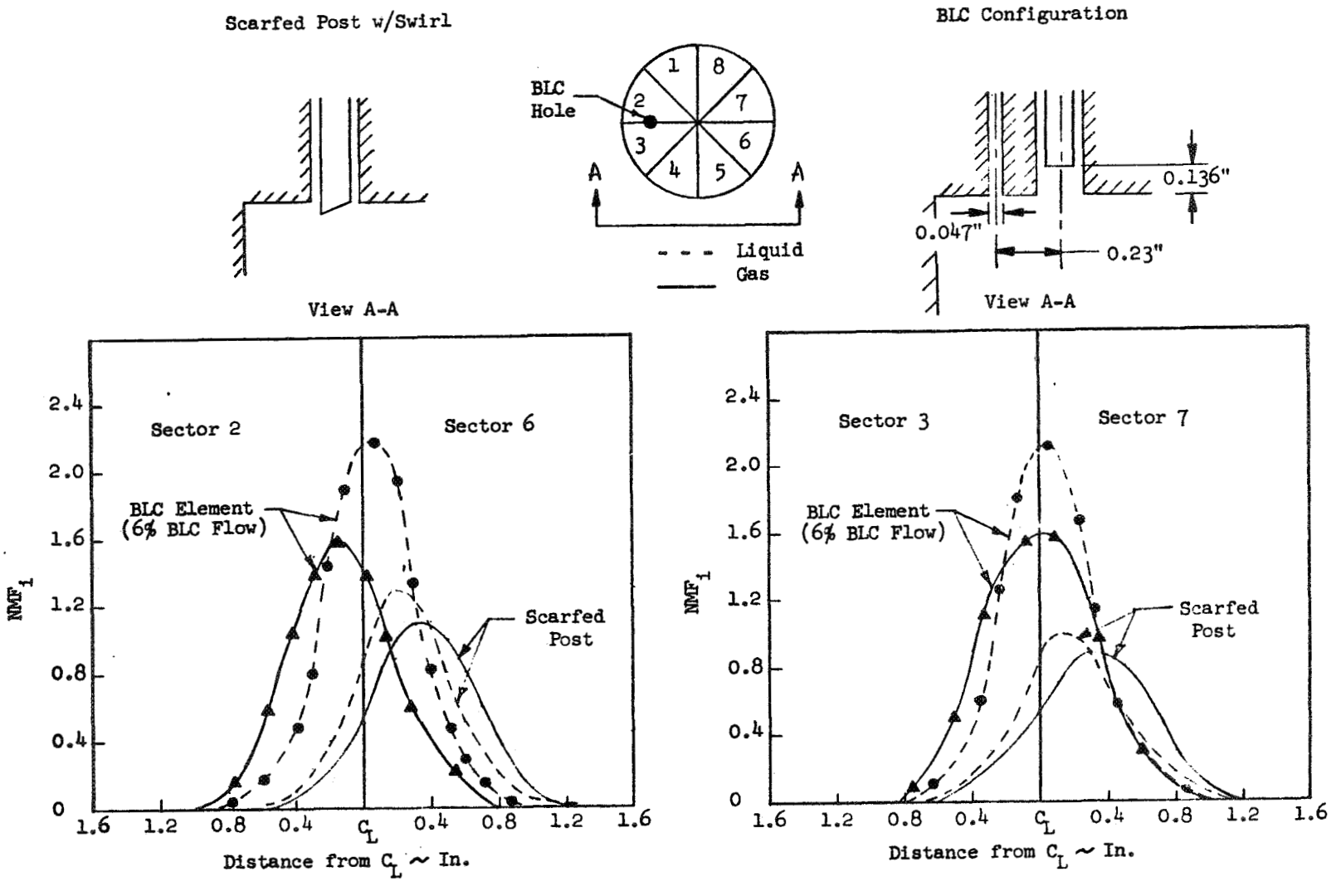

Figure 25. Comparison of Scarfed Post and BLC Element Configurations

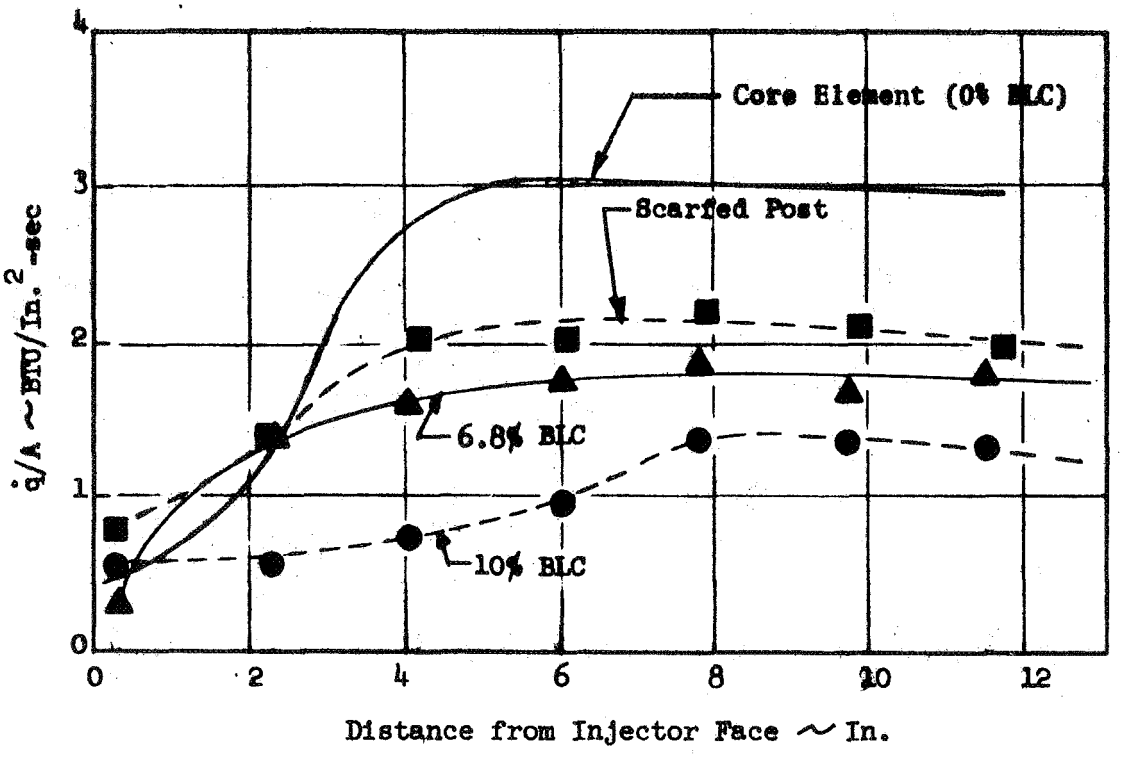

Figure 26. Comparison of Scarfed Post and BLC Heat Flux Levels

The results of the single-element hot-firing data can be physically interpreted in light of the mass flux profiles from the cold-flow experiments. Figure 25 presented (normalized) cold-flow mass flux data for the scarfed post and BLC elements. The flux profiles for the scarfed post element show that the element displaces mass from the wall region but the local wall mixture ratios are higher than the injected mixture ratios. The individual gas and liquid flux profiles for the BLC tests show that liquid distribution is not affected by the showerhead BLC flow. However, the displacement of the gas distribution from the centerline of the element is evident. The resulting characteristics of the BLC flow field include a low wall region mixture ratio, but no reduction in mass fluxes near the wall. From the results of hot-firing experiments, it appears that the low mixture ratios produced by the BLC element were more effective in reducing wall heat fluxes than were the reduced wall mass flux generated by the scarfed post with swirl element.

The results (see Fig. 26) from the single-element hot-firing tests showed that reducing chamber wall zone mixture ratio was more effective in reducing heat flux levels than reducing wall zone mass flux levels. Thus, local wall zone mixture ratios of the peripheral and core elements were correlated with measured wall heat flux rates. Local wall zone mixture rates for the peripheral elements were determined by integrating the mass flux profiles shown in Fig. 25. Only the profiles from Sectors 2 and 3 were integrated since those regions comprise the wall region in the single-element chamber. For the "core" element, wall zone mixture ratio was taken as the injected mixture ratio because, at the test conditions, mixing levels were approximately 98%.

Figure 27 presents the results of the correlation analysis plotted as average chamber wall heat flux as a function of wall zone mixture ratio. Average chamber wall heat fluxes were determined by integrating the heat flux profiles from the injector to the start of nozzle convergence. The average chamber wall heat flux was found to decrease with wall zone mixture ratio. In addition, Fig. 27 shows that employing "peripheral" elements instead of "core" elements in the wall zone of an injector can result in significant reductions in chamber heat flux levels.

Chamber Wall Heat Flux - Full-Scale Injector. Local values of chamber wall heat flux were determined with the full-scale (3000 lbf) coaxial injector of Ref. 2. Figure 28 presents typical chamber heat flux profiles which show the effect of BLC flow. Also shown in Fig. 28 are injector face heat flux levels which were determined during the parametric tests. The data were reduced at a time ($\simeq$2.7 seconds in 3-second test) during the run where the inner chamber wall temperature was calculated (based on measured outer wall temperatures) to be approximately 1000 F. Thus, the chamber wall heat data are comparable with regeneratively cooled chamber data with wall temperatures on the order of 1000 F. As expected, the BLC flow was found to be most effective near the injector end of the chamber. Heat flux levels in the convergent section and nozzle throat were found to be independent of percentage of BLC flow. Note, however, that increasing the percentage of BLC flow from 0 to 9% resulted in a 50% reduction in average chamber wall heat flux. All experiments were conducted in a L* = 40 inches, ε_c = 3:1 chamber.

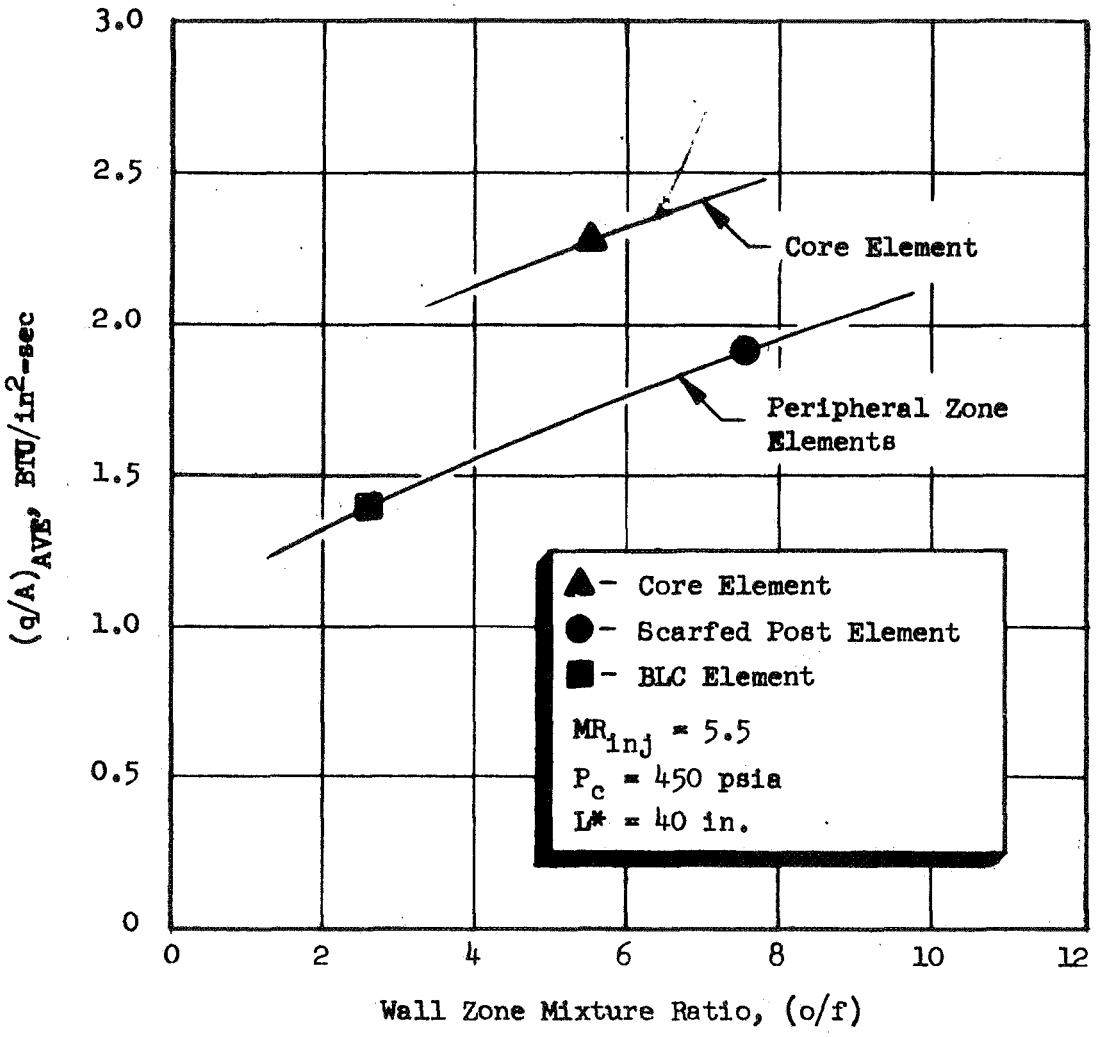

Figure 27. Correlation of Cold-Flow Wall Mixture Ratios With Hot-Fire Average Heat Flux Levels (Injector Face to Start of Nozzle Convergence)

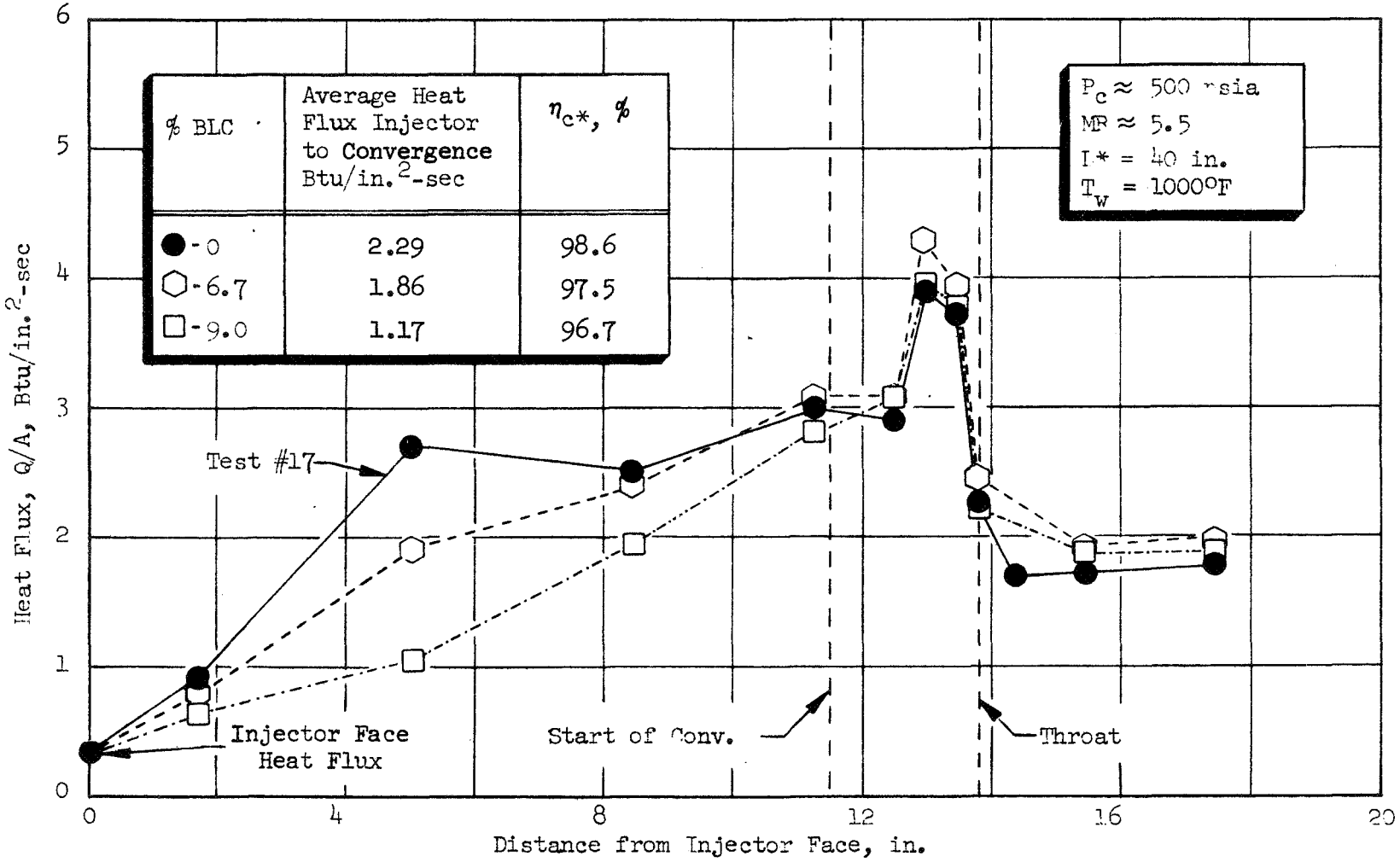

Figure 28. Chamber Heat Flux Profiles as a Function of BLC Flowrate

Correlation of Full-Scale/Single-Element Heat Flux Data. The heat flux data of the full-scale firings and single-element BLC element hot-firing were compared to determine the relationship between single-element and full-scale chamber heat flux characteristics. Both test series were conducted in L* = 40 inches, ε_c = 3:1 chambers. The chamber heat flux levels were averaged by integrating the local heat fluxes from the injector face to the start of nozzle convergence. Figure 29 presents the results of the analysis for various levels of BLC flow-rate. Based on the data of Fig. 29 it appears that single-element hot-fire data can be employed to predict full-scale chamber heat flux data in the chamber region upstream of the start of nozzle convergence.

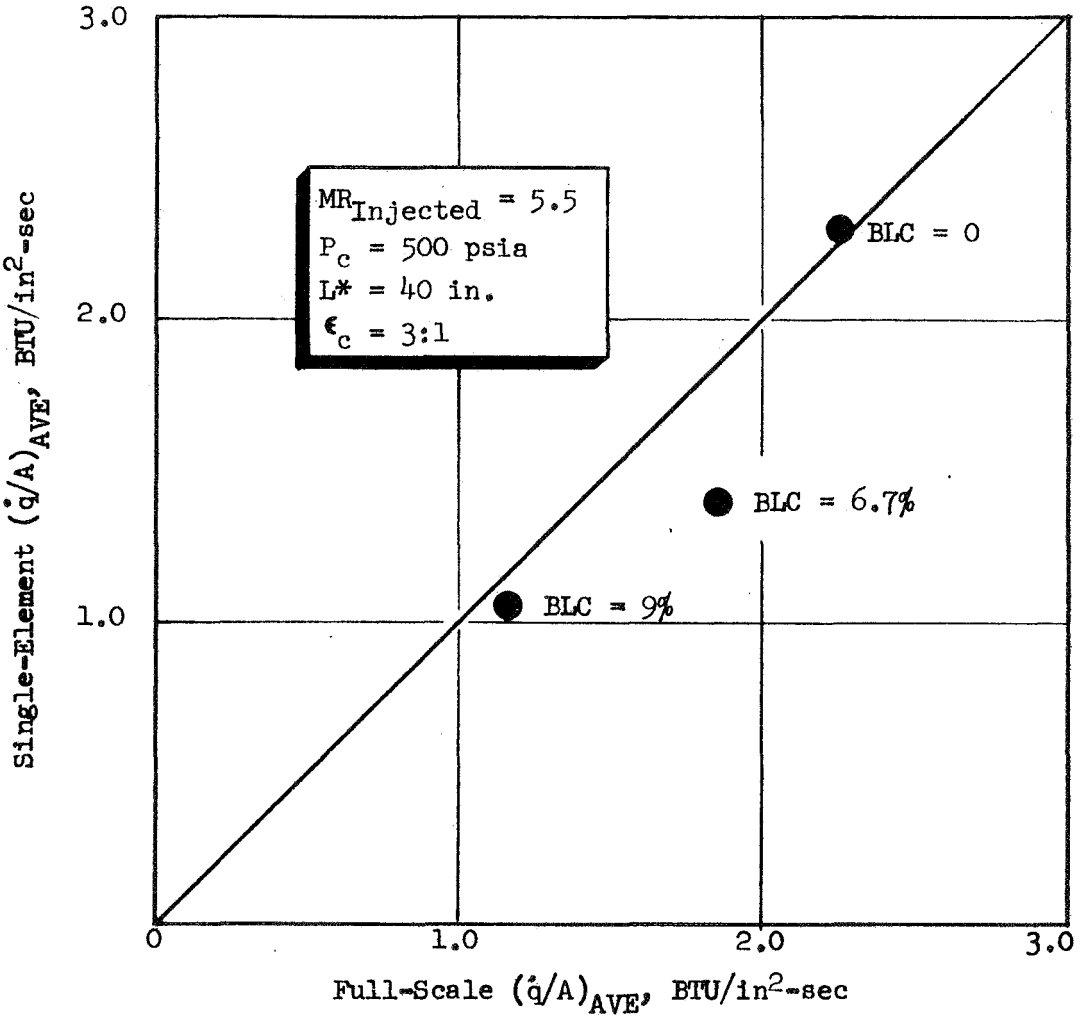

Figure 29. Correlation of Average (Injector to Start of Convergence) Chamber Wall Heat Flux Levels for Single-Element and Full-Scale Hot Firings

5.0 CONCLUDING REMARKS

5.1 COLD-FLOW INJECTOR MODELING TECHNIQUES

The gas/liquid mixing facility/techniques that were developed on this program and Contract NAS3-12001 (Ref. 5) have been shown to be a powerful tool for the rational design of injectors. In particular, the pressurized single-element experiments provided valuable design criteria not only for mixing levels but also resulting mass flow and mixture ratio distributions (chamber compatibility). Cold-flow data were employed to define element design criteria for both high-performance and control of chamber wall heat flux levels.

Perhaps the most valuable gain from the cold-flow testing is the physical insight into how the gas and liquid flow patterns are influenced by changes in element design and operating conditions. Often very small dimensional changes in the design can substantially alter the mass flux and mixture ratio patterns. An application of this information was the revelation that a slight rotation ($\sim$20 degrees) of the like-doublet peripheral injector elements with respect to the chamber wall resulted in placement of the lowest mixture ratio (and, therefore, coolest) gas streams along the chamber wall (Ref. 1). Additionally, experiments with coaxial peripheral elements showed that the cold-flow techniques can provide detailed flow field information which result from subtle change in element design. As an example, the addition of a small BLC hole adjacent to coaxial element can alter significantly the resulting wall zone gas flow field (Ref. 2).

5.2 APPLICATION OF RESULTS TO OTHER PROPELLANT SYSTEMS

The hot-fire and cold-flow data from this study can be employed as guidelines for design of high-performance, chamber-compatible injectors for other gas/liquid propellant combinations. For like-doublet element injectors, propellant mixing and control of chamber heat flux levels (propellant distribution) has been shown to be primarily a function of geometric element design parameters (fan spacing, fan inclination angle, etc.). The oxidizer/fuel injected momentum ratio influenced performance to a lesser degree over the range investigated (0.25 to 2). However, caution should be exercised when applying these data to propellant combinations whose elements operate in ranges considerably different than those employed in this study. To obtain good quantitative design guidance, the recommended approach would be to apply the cold-flow propellant distribution measurement techniques and combustion models developed and verified under this program directly to the propellant and design requirements of interest.

The correlated cold-flow data for circular coaxial elements, presented in Fig. 8 and 9, can be employed to determine element mixing and atomization levels for other gas/liquid propellant combinations (i.e., LOX/GH_2, LOX/propane, etc.). In addition, the correlation of chamber wall heat flux versus chamber wall mixture ratio (Fig. 27) can be employed as a guide in designing elements for enhanced injector/chamber compatibility.

As noted previously, caution must be exercised when applying these data to propellant combinations whose coaxial elements will operate in ranges considerably

different than those employed in this study. Specifically, coaxial elements employing LOX/GH_2 normally operate with significantly higher gas gap velocities ($V_g \approx 2000$ to 3000 ft/sec) than those using methane ($V_g \approx 300$ to 500 ft/sec). In addition, LOX/GH_2 elements generally have larger gas gap heights than those reported herein ($h \approx 0.018$ inch). Cold-flow studies currently underway at Rocketdyne with LOX/GH_2 coaxial elements indicate that the cold-flow data generated in this study may not be directly applicable to LOX/GH_2. However, injector designers concerned with propellants which operate with similar injection characteristics (i.e., LOX/propane) should be able to utilize the results of this study directly.

6.0 DESIGN EXAMPLE

To illustrate the use of the data presented in this report for gas/liquid injector design, design examples are presented herein. High-performance, chamber-compatible circular coaxial and like-doublet injector designs are formulated. Detailed (specific) designs are presented for high performance. The basic approach to be used to attain chamber compatibility is illustrated.

6.1 DESIGN APPROACH

Rational design of rocket engine components using fundamental engineering principles requires a basic understanding of combustion and its relationship to the physical processes (propellant mixing/atomization) that control it.

Consequently, prior to applying experimentally developed mixing/atomization design correlations to the design of an injector-thrust chamber combination, analytical studies should be conducted to define the effects of propellant atomization and mixing on performance as a function of chamber geometry/operating conditions. Results of these analytical studies will provide a definition of injector and thrust chamber design requirements. These performance calculations can be made using vaporization rate-limited and distribution-limited computer programs similar to those employed at Rocketdyne (Ref. 1 through 5).

Once the overall mixing and drop size requirements have been established the injector may be designed using existing mixing/atomization correlations. Design correlations exist for both high performance (i.e., injector core elements) and chamber-compatible (i.e., peripheral zone) elements. Caution should be exercised when applying existing correlations to propellant combinations whose elements operate in ranges considerably different than those upon which the correlation was developed. To obtain good quantitative design guidance in these cases, the recommended approach would be to apply cold-flow propellant mixing/atomization techniques developed and verified on Contract NAS3-12051 directly to the propellants and design requirements of interest.

Design/operating parameters, and mixing and atomization requirements, are defined in Section 6.2. Subsequently, high-performance like-doublet and coaxial injector design concepts are generated (Sections 6.3 and 6.4). The approach to be used to attain chamber compatibility is presented in Section 6.5.

6.2 DEFINITION OF DESIGN/OPERATING PARAMETERS

For this example, the liquid oxygen/gaseous propane propellant combination was selected. Nominal operating parameters are listed in Table III. In addition, reasonably low chamber heat fluxes are desired.

Dimensions of the thrust chamber were established with the aid of the design/operating parameters in Table III. The chamber diameter is 7.90 inches.

TABLE III. DESIGN/OPERATING PARAMETERS

Propellants	Liquid oxygen (LOX)/gaseous propane (C_3H_8)
Chamber Pressure, psia	150
Total Propellant Flowrate, lbm/sec	13.45
Injected Mixture Ratio	2.9
Fuel Density, lbm/ft^3	1.16
Oxidizer Temperature, R	150
Oxidizer Density, lbm/ft^3	71
Fuel Temperature, R	530
Thrust (sea level), pounds	5000
Chamber Contraction Ratio	2.7:1
Performance Level Target (η_{c^*}), percent	96
Chamber Length, inches	10

6.2.1 Definition of Mixing and Atomization Requirements

Mixing Requirements. Equation 1 was employed in conjunction with a distribution-limited, multi-streamtube analysis to determine the effect of mixing on performance for LOX/C_3H_8 as a function of E_m. Results of this analysis are presented in Fig. 30. This figure defines the level of mixing (E_m) required for any reasonable $\eta_{c^*,mix}$. An E_m of 94 is required for an $\eta_{c^*,mix}$ of 99.

Atomization Requirements. A vaporization rate-limited combustion model was employed to determine the effect of propellant drop size on performance. Results of this analysis are presented in Fig. 31. As noted in this figure, a mass median drop size of approximately 100 microns is required for an $\eta_{c^*,vap}$ of 99 in the 10-inch chamber.

To attain the required performance goal (96-percent c* efficiency), a mixing index (E_m) greater than 90 in conjunction with propellant drop sizes or the order of 100 microns will be required.

6.3 LIKE-DOUBLET INJECTOR DESIGN

A simplified flow schematic for the like-doublet injector optimization process is presented in Fig. 32. The upper portion of this figure is common for both injector types. The design procedure for a like-doublet injector is illustrated in the bottom portion of Fig. 32. Specific injector design details for the like-doublet injector are presented below.

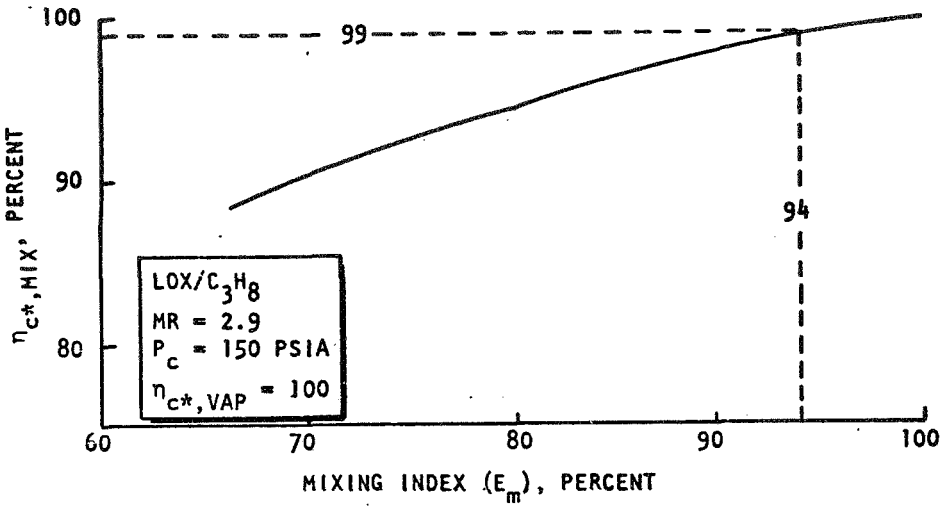

Figure 30. Effect of Propellant Mixing on Performance for LOX/C_3H_8

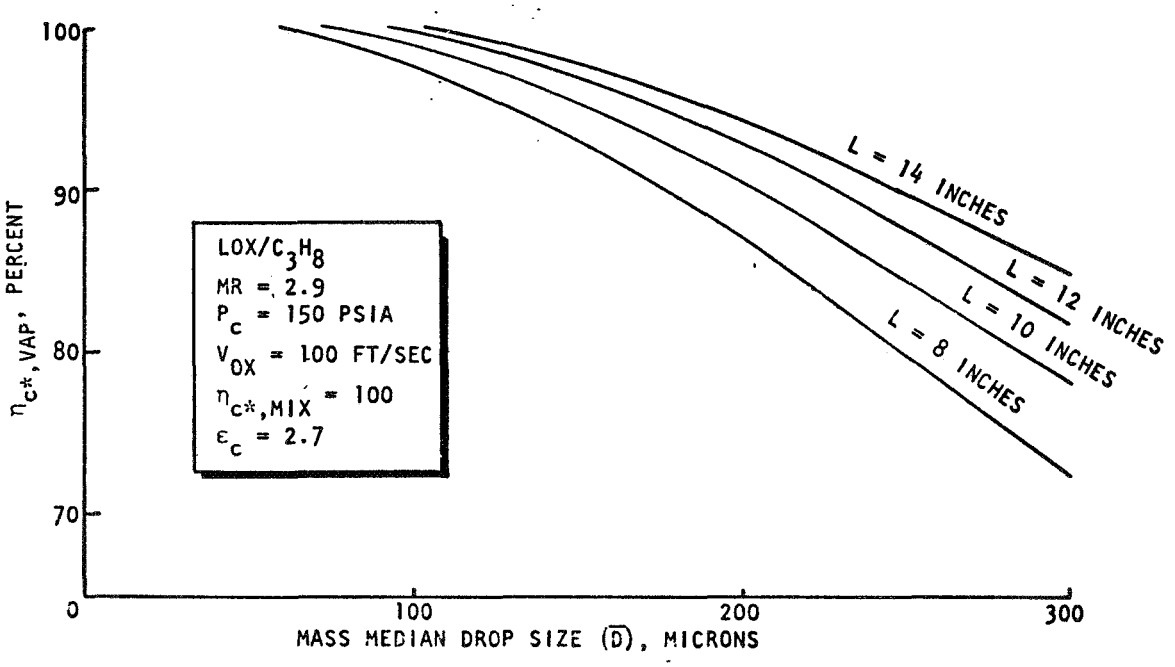

Figure 31. Effect of Propellant Drop Size and Chamber on Performance for LOX/C_3H_8

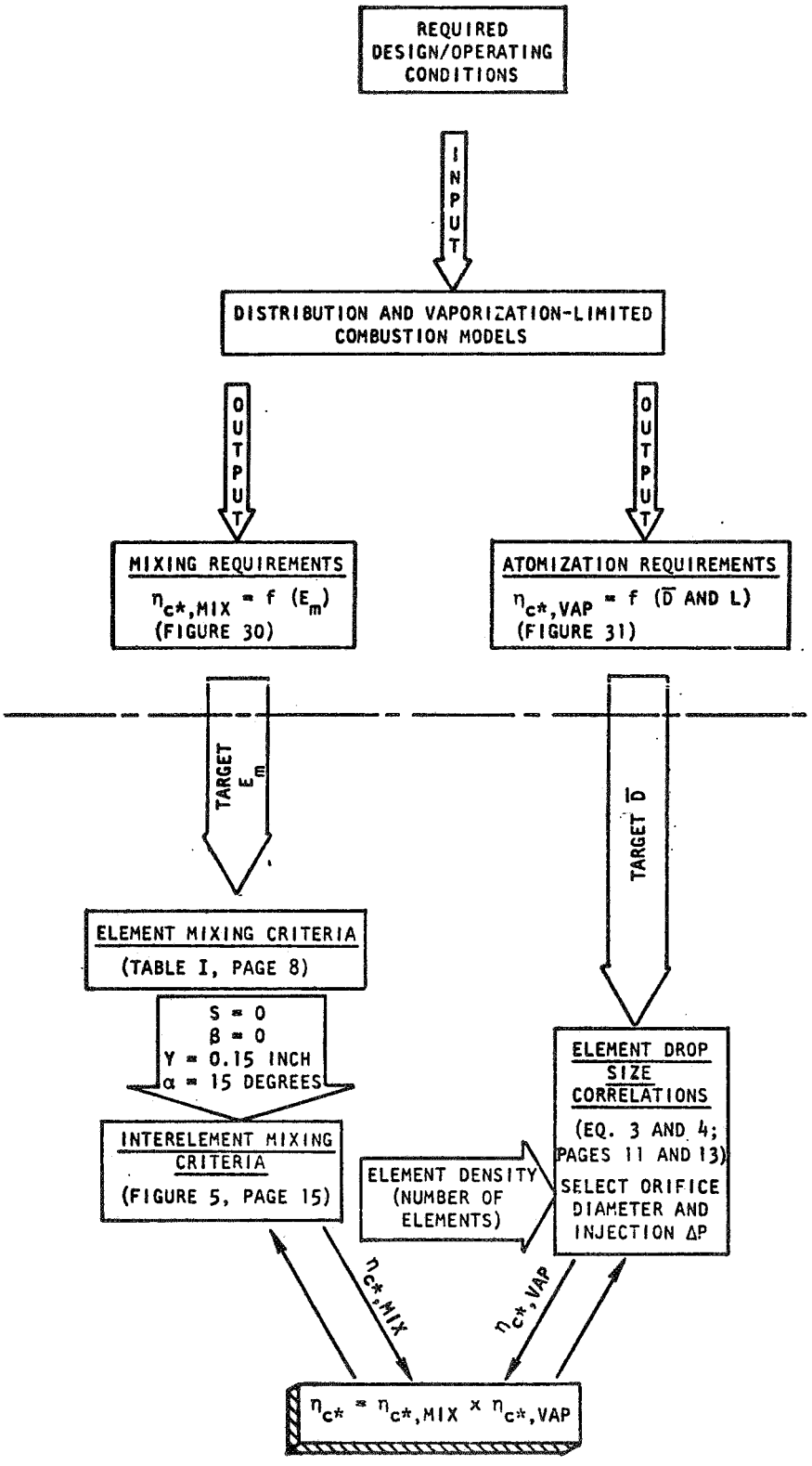

Figure 32. Simplified Flow Schematic for Like-Doublet Injector Optimization (Performance) Process

6.2.1 Basic Element Design

Based on the information in Table I, the basic (high performance) element will have the following design parameters:

Fan Spacing (S) = 0
Impingement Angle (β) = 0
Intra-element Spacing (Y) = 0.15 inch
Fan Inclination Angle (α) = 15 degrees

In addition, the injector should be designed employing the following guidelines:

1. Element placement on the face of the injector should provide essentially uniform propellant mass flux distribution.
2. Oxidizer manifold/feeder passages should be sized so that velocities are less than 10 ft/sec at the design operating conditions and passage entrances should be chamfered or rounded as much as possible to avoid sharp edges. Fuel manifold/feeder velocities should be ~80 ft/sec at the design operating conditions.
3. Oxidizer and fuel orifice L/D's should be ~10. Free stream L/D's for both oxidizer and fuel should be between 3 and 5.
4. The impingement point of the like streams should be ~0.20 inch from the injector face (the included impingement angle of all liquid/gas doublet streams should be 60 degrees).

As noted in Fig. 5 , an element density of ~5.5 elements/sq in. of injector face area is required for an E_m of 92.5. This would result in an $\eta_{c^*,mix}$ of 98.5 for LOX/C_3H_8 (Fig. 30). Since the chamber diameter is 7.90 inches, approximately 270 elements are required to obtain this desired mixing level.

The oxidizer orifice size should be selected, using Eq. 3 and 4, to provide good atomization. The fuel orifice size should be selected to keep the propellant momentum ratio (ℓ/g) between 0.7 and 1.5, and d_f/d_{ox} between 0.5 and 1.0. This is within the range of the experimental data.

Oxidizer drop size is shown plotted as a function of orifice diameter for an injector ΔP of 100 psi (V_{ox} = 91 ft/sec) in Fig. 33. The oxidizer orifice diameter is plotted as a function of the number of elements for several injection pressure drops in Fig. 34. Examination of these figures reveals that use of an oxidizer orifice diemater of 0.0225 inch with an oxidizer injection ΔP of 100 psi will result in an oxidizer D_{30} of ~70 microns ($\overline{D} \cong$ 107 microns).

Vaporization c* efficiency will be 98.5 (Fig. 31). Overall performance would be $\eta_{c^*,mix} \times \eta_{c^*,vap}$ = 98.5 x 98.5 = 97 percent.

A fuel orifice diameter of 0.038 inch ($V_g \cong$ 350 ft/sec) should be employed. This will result in a momentum ratio (ℓ/g) of 0.75 ($d\ell/dg \cong$ 0.61).

Performance could be increased by increasing the element density (i.e., increasing the number of elements) with a resulting increase in $E_m/\eta_{c^*,mix}$. This would

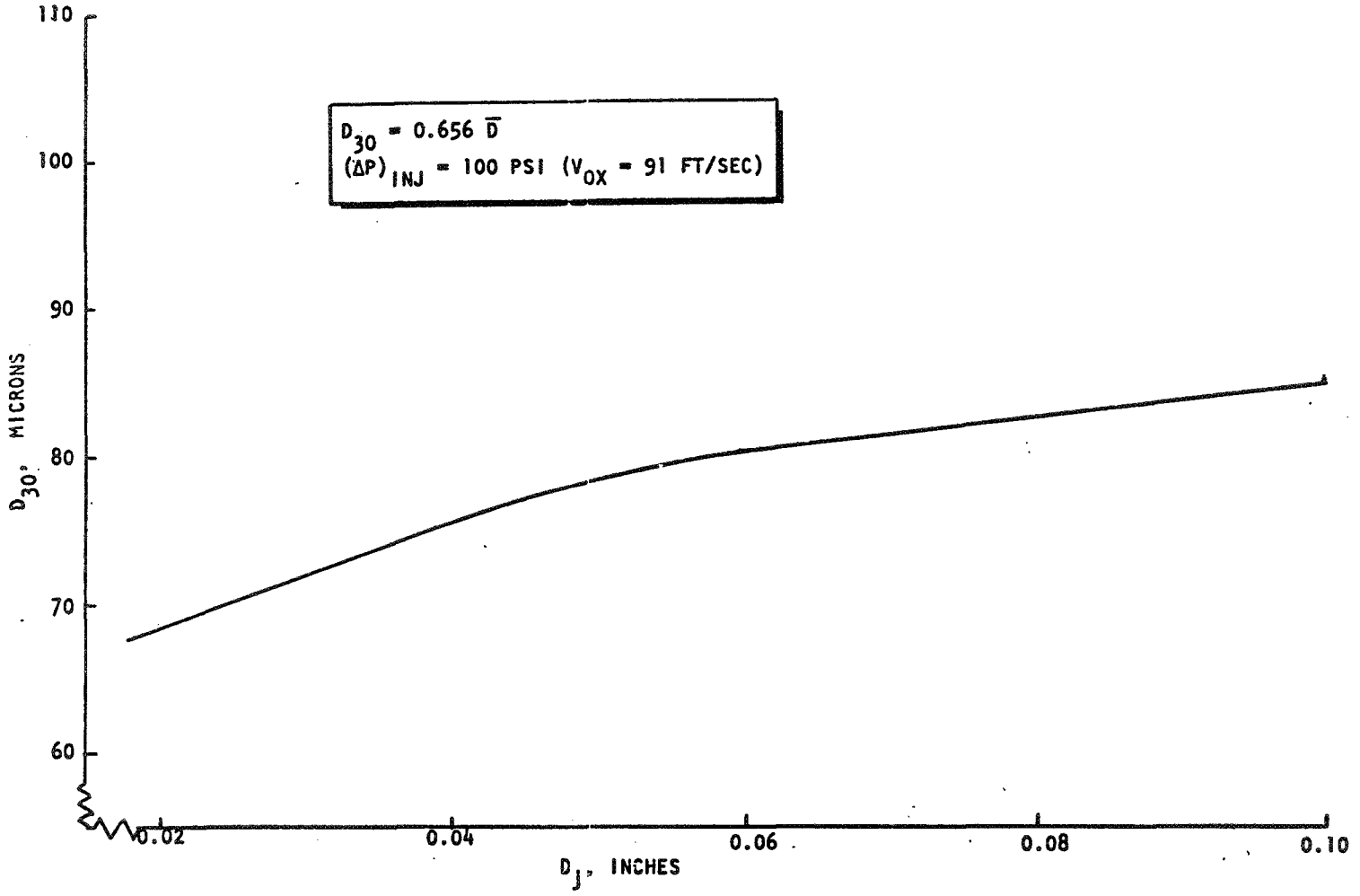

Figure 33. Oxidizer Drop Size as a Function of Orifice Diameter for Injection ΔP of 100 psi

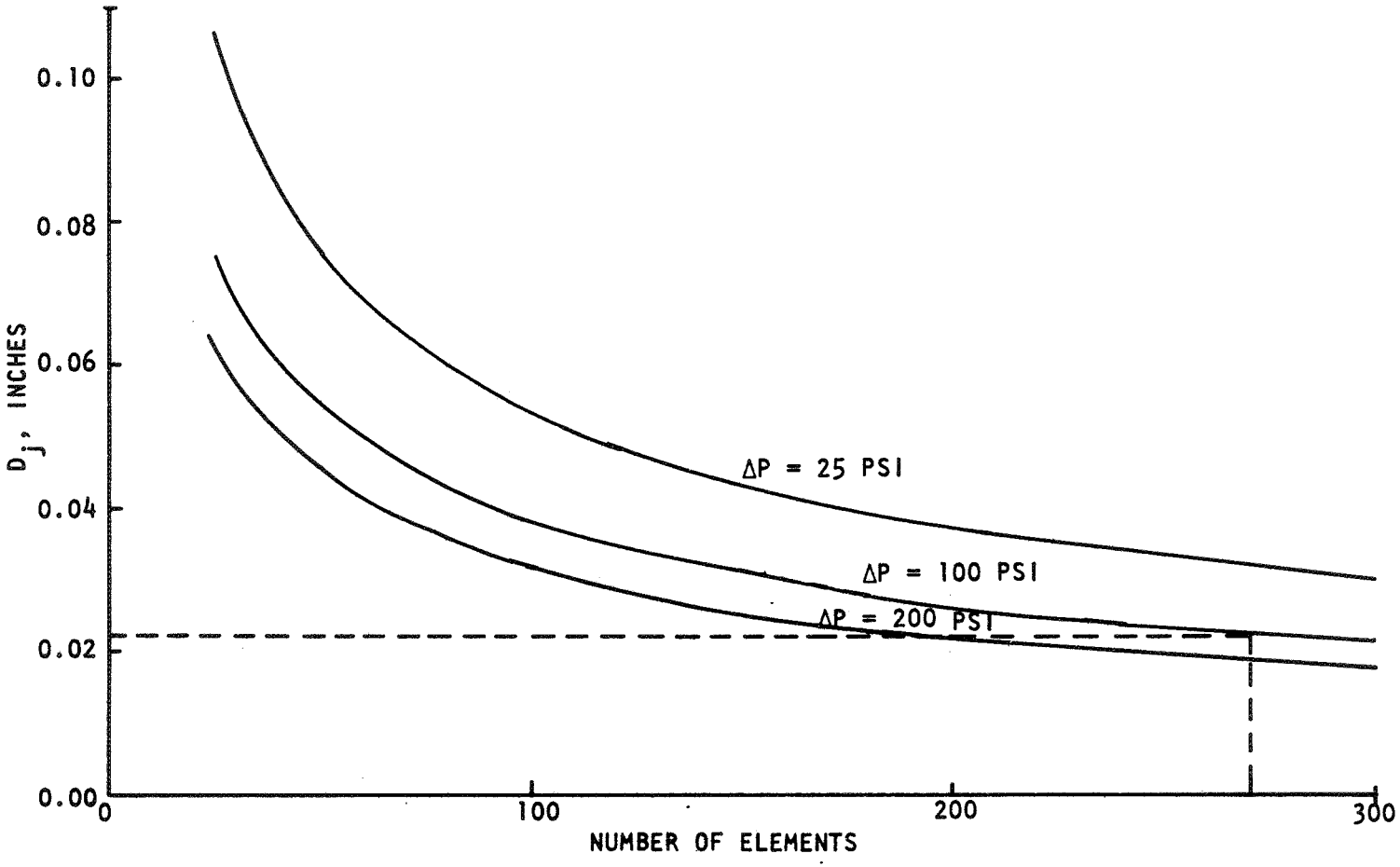

Figure 34. Oxidizer Orifice Diameter as a Function of Number of Elements for Several Injection ΔP's

also result in a smaller oxidizer orifice diameter (ΔP held constant) and somewhat lower $\overline{D}$. However, it would make the injector more complex to fabricate.

6.4 COAXIAL INJECTOR DESIGN

A simplified flow schematic for the coaxial injector optimization process is presented in Fig. 35. The upper position of this figure was discussed in Section 6.3, and is common to both injector types. The design procedure for the coaxial injector is illustrated in the bottom portion of the figure. Specific injector design details for a high-performance coaxial injector are presented below.

6.4.1 Injector Face Pattern

To promote intra-element mixing effects, it is desirable to configure the injector with a relatively high element density. A design layout for this particular application shows that 148 elements may be conveniently arranged in the 7.90-diameter injector face area (see Fig. 36). Thus, the thrust level of each element is equal to 5000/148, or 34 pounds per element. Since this thrust level is similar to that employed in the present study, the cold-flow data can be employed with confidence to predict mixing and vaporization-limited performance.

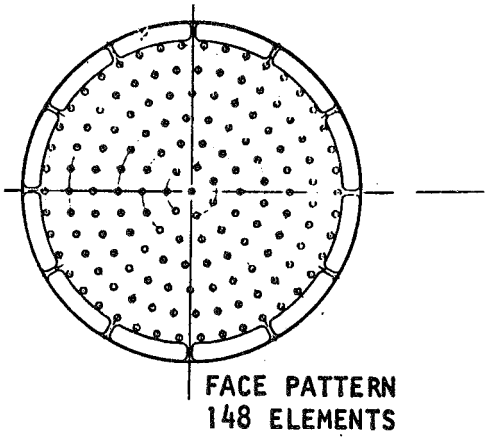

Figure 36. Coaxial Injector Face Pattern

6.4.2 Element Design

Mixing Performance. Based on the correlated single-element cold-flow data of this study optimum mixing was obtained with an element recess of approximately 1 x D_L and with $(\rho_g V_g)^2/MR \cdot V_L$ approximately equal to 2000 lbm^2/ft^5 sec (see Fig. 8).

That value of $(\rho_g V_g)^2/(MR \cdot V_L)$ yields an E_m of approximately 95% which is equivalent to $\eta_{c^*,mix}$ = 99% for the LOX/C_3H_8 system. For the design conditions shown in Table III, this yields the following for the fuel/oxidizer velocity ratio:

$$\frac{(\rho_g V_g)^2}{MR \cdot V_L} = 2000$$

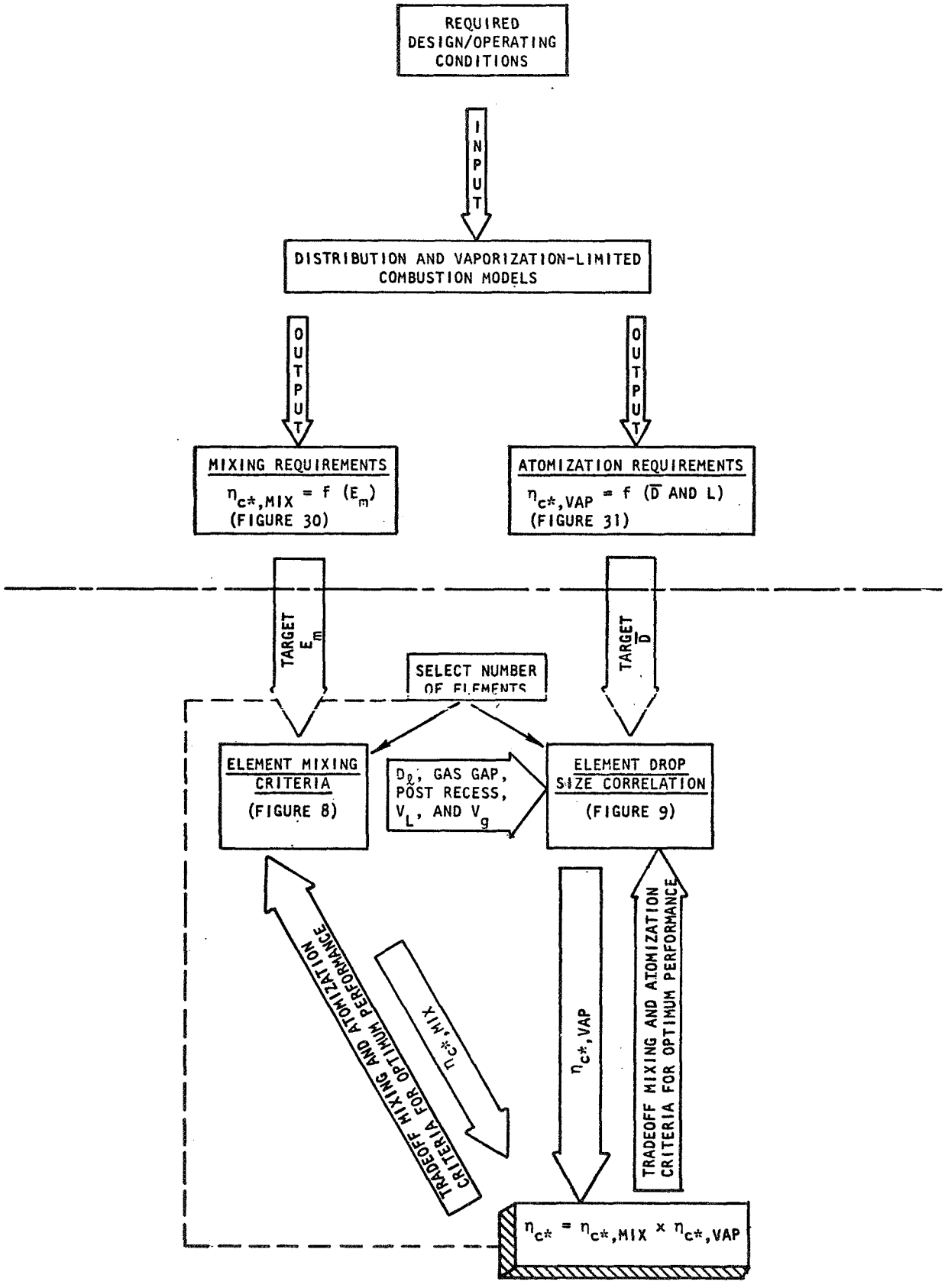

Figure 35. Simplified Flow Schematic for Coaxial Injector Optimization (Performance) Process

or

$$\frac{V_g^2}{V_L} = 4310$$

$$V_g = 65.6 \sqrt{V_L}$$

At the design mixture ratio of 2.9, the total oxidizer and fuel flowrates are 10.00 and 3.45 lbm/sec, respectively. Thus, the respective flowrates per element are:

$$\dot{w}_{ox} = 0.0675 \text{ lbm/sec}$$
$$\dot{w}_{fuel} = 0.0233 \text{ lbm/sec}$$

The correlated cold-flow data (Fig. 8 and 9) were generated with liquid injection velocities on the order of 20ft/sec. Examination of reasonable values for the choice of a liquid jet diameter shows that $D_L = 0.100$ inch yields a liquid injection velocity of 17.6 ft/sec. Thus, for optimum mixing, the gaseous injection velocity is:

$$V_g = 65.6 \sqrt{V_L} = 65.6 \ (4.25)$$

$$V_g = 276 \text{ ft/sec}$$

For a $D_L = 0.100$ inch element, a post wall thickness of 0.020 inch should not present fabrication problems. Thus, the OD of the LOX post and the ID of the fuel annulus is 0.140 inch. Based on the requirement of $V_g = 276$ ft/sec, calculation of the fuel annulus area yields:

$$A_F = \frac{0.0233}{(1.16)(276)} = 0.729 \times 10^{-4} \text{ ft}^2$$

With a post ID equal to 0.140 inch, the required fuel annulus OD is 0.182 inch. Thus, the gas gap height is equal to 0.021 inch. A sketch of this element is shown in Fig. 37.

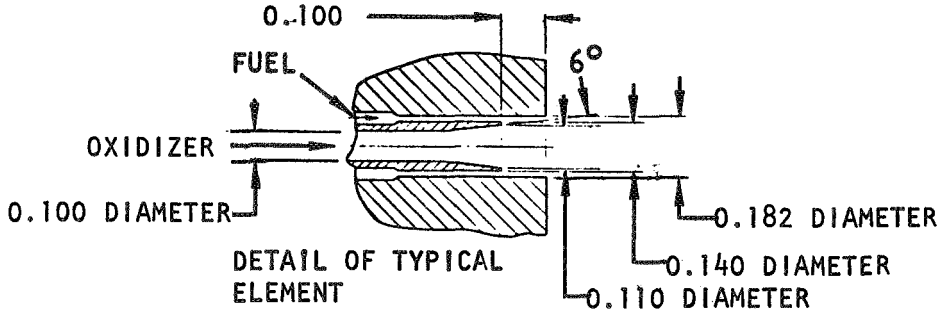

Figure 37. Coaxial Element Configuration

Atomization Performance. At the design conditions, calculations of the predicted mass median drop size are obtained from Fig. 9 . For the element shown in Fig. 37 , which operates at the design conditions:

$$\frac{(V_g - V_L)}{V_L \cdot MR} = \frac{276 - 17.6}{17.6(2.9)} \cong 5.05$$

Based on the correlated (Fig. 9) atomization data, the above value of $(V_g - V_L)/(MR \cdot V_L)$ yields a $\overline{D}/D_L$ value of approximately 0.15. With D_L = 0.100 inch, a predicted mass median drop size (wax)of 380 microns is obtained.

To predict a mean LOX drop size for the hot-fire system, the mean drop size data ($\overline{D}_{wax}$) of Fig. 9 must be corrected for the difference in physical properties of Shell-270 wax and LOX.

The values employed for the respective physical properties of LOX and Shell-270 wax are shown in Table IV.

TABLE IV. PHYSICAL PROPERTIES OF LOX AND WAX

Property	LOX*	Shell-270 Wax**
Viscosity (μ), centipoise	0.23	4.0
Surface Tension (σ), dyne/cm	14.97	17.5
Density (ρ), lbm/ft^3	71.1	47.1

*Data taken from NASA SP-3037, "Handling and Use of Fluorine-Oxygen Mixtures in Rocket Systems"

**Dannenbrink, R. W., Shell Chemical Co., Private Communication, Telecon to L. Zajac, Advanced Programs, Rocketdyne

As indicated, Shell-270 wax simulates reasonably well the surface tension of LOX but differs in density and absolute viscosity.

The correction factor which was employed was based on the work of Ingebo (Ref. 10), i.e.,

$$\overline{D}_{LOX} = \left[\frac{\mu LOX}{\mu wax} \frac{\sigma LOX}{\sigma wax} \frac{\rho wax}{\rho LOX}\right]^{1/4} \overline{D}_{wax}$$

$$= 0.425\ \overline{D}_{wax} = 162 \text{ microns}$$

For $\overline{D}$ = 162 microns, the results of combustion model show that $\eta_{c^*,vap}$ is approximately 94% for a chamber length of 10 inches. Thus, the overall performance of the injector is predicted to be:

$$\eta_{c^*} = 99 \times 94 = 93\%$$

Optimization of Performance. The foregoing example clearly points out that designing an element for optimum mixing (E_m = 95%) does not necessarily mean small vaporization losses will be present. Thus, for a particular design condition, tradeoff studies must be made with respect to element geometry as well as element operating conditions.

In this particular example, the mean drop size can be decreased by increasing the gas gap velocity V_g (i.e., $(V_g - V_L)/MR \cdot V_L$) increases) which can be accomplished by decreasing the gas gap, h. However, as V_g is increased, $(\rho_g V_g)^2/(MR \cdot V_L)$ also increases to values greater than 2000. Consequently, the predicted single-element E_m decreases with an attendant decrease in $\eta_{c^*,mix}$. The need for a tradeoff study to optimize overall performance, η_{c^*}, is obvious.

To obtain an $\eta_{c^*,vap}$ of 98.5% a LOX drop size of 110 microns ($\bar{D}$) is required (Fig. 31). This corresponds to a wax $\bar{D}$ of 259 microns or $\bar{D}/D_L$ of approximately 0.1. Consequently, $(V_g - V_L)/V_L \cdot MR$ should be ~11 (Fig. 9). This will require a V_g of ~590 ft/sec. The corresponding ID of the gas annulus will be 0.160 inch (h = 0.010 inch).

For this configuration, $(\rho_g V_g)^2/MR \cdot V_L \cong 9200$, and $E_m \cong 89$ (Fig. 8), which corresponds to an $\eta_{c^*,mix}$ of 97.5 (Fig. 30). Thus, overall performance = 97.5 x 98.5 ≅ 96.0. Further iteration on the element design (e.g., with a smaller D_ℓ) could possibly result in attainment of higher performance.

The method described in the above paragraphs can be employed as a "first cut" to configure a high-performance injector. However, to optimize the element, the recommended approach would be to apply the cold-flow distribution and atomization techniques in conjunction with the computerized combustion model to optimize the injector directly for the propellants and design requirements of interest.

6.5 CHAMBER HEAT FLUX CONTROL

Peripheral element designs should be such that they will provide acceptably low chamber heat fluxes with minimal performance losses. The basic approach to element designs to achieve this goal is presented herein for both the like-doublet and coaxial elements.

Peripheral zone like-doublet and coaxial element designs are presented and performance losses associated with the designs are estimated.

In general, prior to design of peripheral zone elements, acceptable heat flux levels must be established for the particular test conditions. Available standard heat transfer techniques should then be employed to define expected heat flux levels for the propellant combination and operating conditions of interest. Figures 22 and 27 can then be used as qualitative guides for design of like-doublet and concentric tube peripheral zone elements, respectively, to reduce heat flux levels. For the present example, chamber-compatible designs were selected and performance losses associated with the designs were estimated.

6.5.1 Like-Doublet Pattern

Since the combustion characteristics of LOX/C_3H_8 and FLOX/CH_4 are similar, the chamber heat flux data obtained on Contract NAS3-12051 should provide a reasonable basis for estimation of chamber wall heat flux. Figure [20] presents average chamber wall heat flux for FLOX/CH_4 at 500 and 250 psia. Since chamber heat flux is approximately proportional to $P_c^{0.8}$, heat fluxes for LOX/C_3H_8 at 150-psia chamber pressure may be estimated.

To obtain reduced chamber heat flux levels with minimal performance losses, the elements in the row adjacent to the chamber wall should have a non-zero fan spacing. However, the elements may operate at the same mixture ratio as the "core" elements, since reduced peripheral zone mixture ratio is produced by the non-zero for spacing. The fans in the ring adjacent to the chamber wall should have a fan spacing of 3/16 inch and be aligned with the fans turned ~20 degrees from parallel to the wall, as shown in Fig. 19. This will provide a reduced chamber heat flux level and should not reduce performance by more than 1%.

An estimation of the performance reduction due to the non-zero fan spacing in the peripheral zone elements can be obtained using the equation:

$$(\eta_{c^*,mix}) = (MF)_c \, (\eta_{c^*,mix})_c + (MF)_p \, (\eta_{c^*,mix})_p$$

where

MF = mass fraction

c = core elements

p = peripheral zone elements

The peripheral zone mass flow (or percentage of elements) should be approximately 30% of the total. As noted previously, $\eta_{c^*,mix}$ for the core in this example is 98.5. $\eta_{c^*,mix}$ for the peripheral zone elements is approximately 4% lower than that of the core (page 34). Therefore, $\eta_{c^*,mix}$ for the chamber-compatible injector design would be:

$$0.7 \times 98.5 + 0.3 \times 94.5 \cong 97.5$$

Atomization would remain essentially unchanged. Consequently, overall performance $\cong$ 97.5 x 98.5 = 96.0. This represents approximately a 1% loss in performance due to the chamber-compatible elements.

6.5.2 Coaxial Pattern

Employing a BLC element clnfiguration similar to that of Fig. [25], appreciable chamber heat flux reduction could be obtained with minimal performance losses (~1%, Fig. [28]).

7.0 REFERENCES

1. Falk, A. Y., Space Storable Propellant Performance--Gas/Liquid Like-Doublet Injector Characterization, Final Report, R-8973 (NASA CR-120935), Rocketdyne, a division of Rockwell International, Canoga Park, California, October 1972.

2. Burick, R. J., Space Storable Propellant Performance--Coaxial Injector Characterization, Final Report, R-8973-2 (NASA CR-120936), Rocketdyne, a division of Rockwell International, Canoga Park, California, October 1972.

3. Falk, A. Y., et al., Space Storable Propellant Performance Study, Final Report, R-7677 (NASA CR-72487), Rocketdyne, a division of Rockwell International, Canoga Park, California, November 1968.

4. AFRPL-TR-68-143, Correlation of Spray Injector Parameters With Rocket Engine Performance, R. Dickerson, et al., Rocketdyne, a division of Rockwell International, Canoga Park, California, June 1968.

5. Mehegan, D. F., et al., Investigation of Gas-Augmented Injectors, NASA CR-72703, Rocketdyne, a division of Rockwell International, Canoga Park, California, September 1970.

6. Contract NAS7-304, Chamber Technology for Space Storable Propellants, Third Interim Report, Rocketdyne, a division of Rockwell International, Canoga Park, California, May 1967.

7. Technical Documentary Report No. TR-65-107, Performance Characteristics of Compound "A"/Hydrazine Propellant Combinations, Rocketdyne, a division of Rockwell International, Canoga Park, California, May 1965.

8. Rupe, J. H., The Liquid Phase Mixing of a Pair of Impinging Streams, Progress Report No. 20-195, Jet Propulsion Laboratory, Pasadena, California, 6 August 1953.

9. Zajac, L. J., Correlation of Spray Dropsize Distributions and Injector Variables, R-8455, Rocketdyne, a division of Rockwell International, Canoga Park, California, November 1971.

10. Ingebo, R. E., Dropsize Distributions for Impinging Jet Breakup in Airstreams Simulating the Velocity Condition in Rocket Combustors, NACA TN 4222, 1958.

APPENDIX A

DISTRIBUTION LIST (CONTRACT NAS3-12051)

Report Copies R	D	Recipient	Designee
		National Aeronautics & Space Administration Lewis Research Center 21000 Brookpark Road Cleveland, Ohio 44135	
1		Attn: Contracting Officer, MS 500-513	
5		E. A. Bourke, MS 500-203	
1		Technical Report Control Office, MS 5-5	
1		Technology Utilization Office, MS 3-16	
2		AFSC Liaison Office, 501-3	
2		Library	
1		Office of Reliability & Quality Assurance, MS 500-111	
1		J. W. Gregory Chief, MS 500-203	
10		L. H. Gordon Project Manager, MS 509-209	
1		E. M. Krawczonek, MS 500-204	
1		J. P. Wanhainen, MS 500-208	
1		N. P. Hannum, MS 500-208	
1		Director, Shuttle Technology Office, RS Office of Aeronautics & Space Technology NASA Headquarters Washington, D.C. 20546	
2		Director Space Prop. and Power, RP Office of Aeronautics & Space Technology NASA Headquarters Washington, D.C. 20546	
1		Director, Launch Vehicles & Propulsion, SV Office of Space Science NASA Headquarters Washington, D.C. 20546	
1		Director, Materials & Structures Div., RW Office of Aeronautics & Space Technology NASA Headquarters Washington, D.C. 20546	
1		Director, Advanced Manned Missions, MT Office of Manned Space Flight NASA Headquarters Washington, D.C. 20546	

Report Copies R	D	Recipient	Designee
27		National Technical Information Service Springfield, Virginia 22151	
1		National Aeronautics & Space Administration Ames Research Center Moffett Field, California 94035 Attn: Library	Hans M. Mark Mission Analysis Division
1		National Aeronautics & Space Administration Flight Research Center P.O. Box 273 Edwards, California 93523 Attn: Library	
1		Director, Technology Utilization Division Office of Technology Utilization NASA Headquarters Washington, D.C. 20546	
1		Office of the Director of Defense Research & Engineering Washington, D.C. 20301 Attn: Office of Asst. Dir. (Chem. Technology)	
2		NASA Scientific and Technology Information Facility P.O. Box 33 College Park, Maryland 20740 Attn: NASA Representative	
1		Nation Aeronautics & Space Administration Goddard Space Flight Center Greenbelt, Maryland 20771 Attn: Library	Merland L. Moseson Code 620
1		National Aeroanutics & Space Administration John F. Kennedy Space Center Cocoa Beach, Florida 32931 Attn: Library	Dr. Kurt H. Debus
1		National Aeronautics & Space Administration Langley Research Center Langley Station Hampton, Virginia 23365 Attn: Library	E. Cortwright Director

Report Copies R	D	Recipient	Designee
1		National Aeronautics & Space Administration Manned Spacecraft Center Houston, Texas 77001 Attn: Library	J. G. Thiobodaux, Jr. Chief, Propulsion & Power Division
1		National Aeronautics & Space Administration George C. Marshall Space Flight Center Huntsville, Alabama 35912 Attn: Library	Hans G. Paul Leon J. Hastings James Thomas Dale Burrows I. G. Yates Clyde Nevins J. Blumrich
1		Jet Propulsion Laboratory 4800 Oak Grove Drive Pasadena, California 91103	Henry Burlage, Jr. Duane Dipprey
	1	Attn: Library	R. Kushida
1		Defense Documentation Center Cameron Station Building 5 5010 Duke Street Alexandria, Virginia 22314 Attn: TISIA	
1		RTD (RTNP) Bolling Air Force Base Washington, D.C. 20332	
1		Arnold Engineering Development Center Air Force Systems Command Tullahoma, Tennessee 37389 Attn: Library	Dr. H. K. Doetsch
1		Advanced Research Projects Agency Washington, D.C. 20525 Attn: Library	
1		Aeronautical Systems Division Air Force Systems Command Wright-Patterson Air Force Base Dayton, Ohio Attn: Library	D. L. Schmidt Code ARSCNC-2
1		Air Force Missile Test Center Patrick Air Force Base, Florida Attn: Library	L. J. Ullian

Report Copies R	D	Recipient	Designee
1		Air Force Systems Command Andrews Air Force Base Washington, D.C. 20332 Attn: Library	Capt. S. W. Bowen SCLT
1		Air Force Rocket Propulsion Laboratory (RPR) Edwards, California 93523 Attn: Library	
1		Air Force Rocket Propulsion Laboratory (RPM) Edwards, California 93523 Attn: Library	
1		Air Force FTC (FTAT-2) Edwards Air Force Base, California 93523 Attn: Library	Donald Ross
1		Air Force Office of Scientific Research Washington, D.C. 20333 Attn: Library	SREP, Dr. J. F. Masi
1		Space & Missile Systems Organization Air Force Unit Post Office Los Angeles, California 90045 Attn: Technical Data Center	
1		Office of Research Analyses (OAR) Holloman Air Force Base, New Mexico 88339 Attn: Library RRRD	
1		U.S. Air Force Washington, D.C. Attn: Library	Col. C. K. Stambaugh Code AFRST
1		Commanding Officer U.S. Army Research Office (Durham) Box CM, Duke Station Durham, North Carolina 27706 Attn: Library	
1		U.S. Army Missile Command Redstone Scientific Information Center Redstone Arsenal, Alabama 35808 Attn: Document Section	Dr. W. Wharton

Report Copies R	D	Recipient	Designee
1		Bureau of Naval Weapons Department of the Navy Washington, D.C. Attn: Library	J. Kay Code RTMS-41
1		Commander U.S. Naval Missile Center Point Mugu, California 93041 Attn; Technical Library	
1		Commander U.S. Naval Weapons Center China Lake, California 93557 Attn: Library	
1		Commanding Officer Naval Research Branch Office 1030 E. Green Street Pasadena, California 91101 Attn: Library	
1		Director (Code 6180) U.S. Naval Research Laboratory Washington, D.C. 20390 Attn: Library	H. W. Carhart J. M, Krafft
1		Picatinny Arsenal Dover, New Jersey 07801 Attn: Library	I. Forsten
1		Air Force Aero Propulsion Laboratory Research & Technology Division Air Force Systems Command United States Air Force Wright-Patterson AFB, Ohio 45433 Attn: APRP (Library)	R. Quigley C. M. Donaldson
1		Electronics Division Aerojet-General Corporation P.O. Box 296 Azusa, California 91703 Attn: Library	W. L. Rogers

Report Copies R	D	Recipient	Designee
1		Space Division Aerojet-General Corporation 9200 East Flair Drive El Monte, California 91734 Attn: Library	S. Machlawski
1		Aerojet Ordance and Manufacturing Aerojet-General Corporation 11711 South Woodruff Avenue Fullerton, California 90241 Attn: Library	
1		Aerojet Liquid Rocket Company	R. Stiff
	1	P.O. Box 15847	D. L. Kors
	1	Sacramento, California 95813	D. Calhoon
	1	Attn: Technical Library 2484-2015A	J. Ito
1		Aeronutrionic Division of Philco Ford Corp. Ford Road Newport Beach, California 92663 Attn: Technical Information Department	Dr. L. H. Linder
1		Aerospace Corporation 2400 E. El Segundo Blvd. Los Angeles, California 90045 Attn: Library-Documents	J. G. Wilder
1		Arthur D. Little, Inc. 20 Acorn Park Cambridge, Massachusetts 02140 Attn: Library	A. C. Tobey
1		Astropower Laboratory McDonnel-Douglas Aircraft Company 2121 Paularino Newport Beach, California 92163 Attn: Library	
1		ARO, Incorporated Arnold Engineering Development Center Arnold AF Station, Tennessee 37389 Attn: Library	
1		Susquehanna Corporation Atlantic Research Division Shirley Highway & Edsall Road Alexandria, Virginia 22314 Attn: Library	

Report Copies R	D	Recipient	Designee
1		Beech Aircraft Corporation Boulder Facility Box 631 Boulder, Colorado Attn: Library	Douglas Pope
1		Bell Aerosystems, Inc. Box 1 Buffalo, New York 14240 Attn: Library	T. Reinhardt W. M. Smith J. M. Senneff
	1		
1		Instruments & Life Support Division Bendix Corporation P.O. Box 4508 Davenport, Iowa 52808 Attn: Library	W. M. Carlson
1		Boeing Company Space Division P.O. Box 868 Seattle, Washington 98124 Attn: Library	J. D. Alexander C. F. Tiffany
1		Chemical Propulsion Information Agency Applied Physics Laboratory 8621 Georgia Avenue Silver Spring, Marlyand 20910	Tom Reedy
1		Chrysler Corporation Missile Division P.O. Box 2628 Detroit, Michigan Attn: Library	John Gates
1		Chrysler Corporation Space Division P.O. Box 29200 New Orleans, Louisiana 70129 Attn: Librarian	
1		Curtiss-Wright Corporation Wright Aeronautical Division Woodridge, New Jersey Attn: Library	G. Kelley

Report Copies R	D	Recipient	Designee
1		University of Denver Denver Research Institute P.O. Box 10127 Denver, Colorado 80210 Attn: Security Office	
1		Fairchild Stratos Corporation Aircraft Missiles Division Hagerstown, Maryland Attn: Library	
1		Research Center Fairchild Hiller Corporation Germantown, Maryland Attn: Library	Ralph Hall
1		General Dynamics/Convair P.O. Box 1128 San Diego, California 92112 Attn: Library	Frank Dore
1		Missiles and Space Systems Center General Electric Company Valley Forge Space Technology Center P.O. Box 8555 Philadelphia, Pa. 19101 Attn: Library	A. Cohen F. Schultz
1		General Electric Company Flight Propulsion Lab. Department Cincinnati, Ohio Attn: Library	D. Suichu Leroy Smith
1		Grumman Aircraft Engineering Corporation Bethpage, Long Island, New York Attn: Library	Joseph Gavin
1		Hercules Powder Company Allegheny Ballistics Laboratory P.O. Box 210 Cumberland, Maryland 21501 Attn: Library	
1		IIT Research Institute Technology Center Chicago, Illinois 60616 Attn: Library	C. K. Hersh

Report Copies R	D	Recipient	Designee
1		Kidde Aer-Space Division Water Kidde & Company, Inc. 567 Main Street Belleville, N. J. 07109	R. J. Hanville
1		Ling-Temco-Vought Corporation P.O. Box 5907 Dallas, Texas 75222 Attn: Library	
1		Lockheed Missiles and Space Company P.O. Box 504 Sunnyvale, California 94087 Attn: Library	
1		Lockheed Propulsion Company P.O. Box 111 Redlands, California 92374 Attn: Library, Thackwell	H. L. Thackwell
1		Marquardt Corporation 16555 Saticoy Street Box 2013 - South Annex Van Nuys, California 91409	L. R. Bell Jr.
1		Denver Division Martin-Marietta Corporation P.O. Box 179 Denver, Colorado 80201 Attn: Library	Dr. Morganthaler F. R. Schwartzberg
1		Western Division McDonnell Douglas Astronautics 5301 Bolsa Ave. Huntington Beach, California 92647 Attn: Library	R. W. Hallet G. W. Burge P. Klevatt
1		McDonnell Douglas Aircraft Corporation P.O. Box 516 Lambert Field, Missouri 63166 Attn: Library	R. A. Herzmark
1		Space & Information Systems Division North American Rockwell 12214 Lakewood Blvd. Downey, California Attn: Library	

Report Copies R	D	Recipient	Designee
1		Northrop Space Laboratories 3401 West Broadway Hawthorne, California Attn: Library	Dr. Wm. Howard
1		Purdue University Lafayette, Indiana 47907 Attn: Library (Technical)	Dr. Bruce Reese
1		Rocket Research Corporation Willow Road at 116th Street Redmond, Washington 98052 Attn: Library	F. McCullough, Jr.
1		Stanford Research Institute 333 Ravenswood Avenue Menlo Park California 94023 Attn: Library	Dr. Gerald Marksman
1		TRW Systems, Inc.	D. H. Lee
	1	1 Space Park	H. Burge
	1	Redondo Beach, California 90278 Attn: Tech. Lib. Doc. Acquisitions	W. A. Carter
1		United Aircraft Corporation Corporation Library 400 Main Street East Hartford, Connecticut 06108 Attn: Library	Dr. David Rix Erle Martin Frank Owen Wm. E. Taylor
1		United Aircraft Corporation	R. J. Coar
	1	Pratt & Whitney Division Florida Research & Development Center	A. Masters Dr. Schmitke
	1	P.O. Box 2691	T. E. Bailey
	1	West Palm Beach, Florida 33402 Attn: Library	P. Mitchel
1		United Aircraft Corporation United Technology Center P.O. Box 358 Sunnyvale, California 94038 Attn: Library	Dr. David Altman
1		Garret Corporation AiResearch Division Phoenix, Arizona, 85036 Attn: Library	R. Bullock J. R. Erwin